Kaon and pion production in relativistic heavy-ion collisions

M. Wagner, A. B. Larionov,* and U. Mosel
Institut für Theoretische Physik, Universität Giessen, D-35392 Giessen, Germany
(Received 4 November 2004; published 31 March 2005)

The Boltzmann-Uehling-Uhlenbeck (BUU) transport model is applied to study strangeness and pion production in nucleus-nucleus collisions. Starting from proton induced reactions, we further investigate Si+Au, Au+Au, and Pb+Pb collisions in the energy range between 2 and 40A GeV and compare the results with data and other transport calculations. The $q\bar{q}$-annihilation, or resonance, channel simulated by the string model in meson-nucleon collisions at $\sqrt{s} > 2$ GeV is introduced. The importance of this channel for a good description of the proton-nucleus data on K^+ production is demonstrated. We further show that meson-meson collisions contribute significantly to the $K\overline{K}$ production in heavy-ion collisions above 5A GeV and improve the agreement with data on the K^+/π^+ ratio. Finally, we study the influence of in-medium modifications of the FRITIOF model on pion and kaon production.

DOI: 10.1103/PhysRevC.71.034910 PACS number(s): 24.10.Lx, 25.75.−q, 13.85.Ni

I. INTRODUCTION

High-energy heavy-ion collisions offer a unique possibility to study nuclear matter at high densities and temperatures under laboratory conditions. The maximum compression is expected at a beam energy of about 30A GeV. The most intriguing phenomenon that can happen in highly compressed nuclear matter is the transition to the quark-gluon plasma. Pioneering work at large baryon densities was done at the Alternating Gradient Synchrotron (AGS) in Brookhaven, where the energy range up to 15A GeV was explored (see [1] and references therein). The future facility at Gesellschaft für Schwerionenforschung (GSI) will provide beams from 2 up to 40A GeV. An indirect signal for the quark-gluon plasma is believed to be the strangeness enhancement, which was first suggested by Rafelski and Müller [2]. If this is true, the enhancement should then be seen in the most abundant strange particles, the kaons. At the AGS and CERN superproton synchrotron (SPS) energies, the K^+/π^+ ratio was studied, and indeed a maximum in the ratio was found at about 30A GeV [3]. Theoretical calculations with different transport codes—Relativistic Quantum Molecular Dynamics (RQMD) [4,3], Hadron-String Dynamics (HSD) [5], and original quantum molecular dynamics (Ultrarelativistic Quantum Molecular Dynamics; UrQMD) [6]—have recently been performed. These calculations were not able to reproduce the peak in the ratio, which was either at a wrong energy (RQMD, UrQMD) or not present at all (HSD). In the case of HSD and UrQMD, this discrepancy was due to overpredicted pion production, while the kaon yield was well described [6]. With an eye on the planned Compressed Baryonic Matter (CBM) experiment at GSI, it is therefore important to check whether the mentioned difficulties are genuine difficulties in the transport approach or consequences of a particular numerical implementation.

In the present work, we study pion and kaon production at energies of 2–40A GeV within the BUU model [7,8]; we stress that this is a numerical implementation independent of those employed in [3,4,6]. First, we systematically increase the system size and show its effect on particle production. In particular, an analysis of the centrality dependence of the pion and kaon production from Au+Au collisions at 10.7A GeV is performed and compared to the data [9]. Then we study the K^+/π^+ ratio in central Au+Au and Pb+Pb collisions as a function of the beam energy and compare our results to the experimental data and other models. Special emphasis is put on the strangeness production, and we show in detail the most important production mechanisms at different energies.

The structure of the paper is as follows. In Sec. II, we describe our BUU model. In Sec. III, we study the influence of the system size on pion and kaon production. In Sec. IV, we show the excitation functions of pions, kaons, and Λ and Σ hyperons in central heavy-ion collisions. In Sec. V, we discuss a medium modification of the FRITIOF string model and its influence on pion and kaon production. The summary and outlook are given in Sec. VI.

II. THE BUU MODEL

Our calculations are based on the BUU model described in Refs. [7,8]. In the high-energy range ($\sqrt{s} > 2$ GeV) we adopt the treatment of Falter *et al.* [10]. Thus, we eliminate details relating only to the main ingredients and modifications.

The model treats a nucleus-nucleus collision explicitly in time as a sequence of baryon-baryon, meson-baryon, and meson-meson collisions. If not specified explicitly, the calculation is always done in the cascade mode, i.e., particles propagate freely between the two-body collisions. The baryon-baryon collisions at the invariant energy $\sqrt{s} < 2.6$ GeV are treated via a resonance scenario, whereas at $\sqrt{s} > 2.6$ GeV, a FRITIOF string model [11] is applied. In the case of the meson-baryon collisions, the resonance (FRITIOF) model is used at $\sqrt{s} < (>)2$ GeV. In most of the calculations, we use an energy dependent strangeness suppression factor

*On leave from RRC "I.V. Kurchatov Institute," 123182 Moscow, Russia.

 ©2005 The American Physical Society

from Ref. [12]:

$$\gamma \equiv \frac{P(s)}{P(u)} = \begin{cases} 0.3 & \text{for} \quad \sqrt{s} \geqslant 20\ \text{GeV}, \\ 0.4 & \text{for} \quad \sqrt{s} \leqslant 5\ \text{GeV}, \\ 0.433 - \frac{1}{150}\sqrt{s}\ [\text{GeV}]^{-1} & \text{for} \\ \quad 5\ \text{GeV} < \sqrt{s} < 20\ \text{GeV}. \end{cases} \tag{1}$$

Sometimes, we also apply an energy independent strangeness suppression factor $\gamma = 0.3$, which is mentioned explicitly in the text.

The most important modifications are the implementation of the strangeness production channels in meson-meson collisions and the possibility for a baryon and a meson to annihilate into a resonance with an invariant mass of more than 2 GeV, whose decay is simulated by the string model. These two modifications are explained in detail below. In Sec. IV, we show how the meson-meson collisions and the effective resonance channel influence the K^+/π^+ ratio (see Fig. 19).

A. Meson-meson reactions

Our BUU model explicitly propagates π, η, ρ, σ, ω, ϕ, K, and the K^* mesons. Charmed mesons are also included, but they are not relevant for the energies under consideration and thus we do not mention them further. At beam energies up to $2A$ GeV, production of mesons heavier than pions is negligible and the only relevant meson-meson channel of strangeness production is $\pi\pi \leftrightarrow K\overline{K}$, which was included in the earlier version of the BUU model [8]. At higher energies, heavier mesons are produced more abundantly, and therefore one also has to take into account the strangeness production in other meson-meson collisions, e.g., $\pi\rho \leftrightarrow K\overline{K}$. The problem is, however, that the cross sections of these processes are not measured experimentally. In Ref. [13], the cross sections of the processes $\pi\pi \to K\overline{K}$, $\pi\rho \to K\overline{K}$, and $\rho\rho \to K\overline{K}$ were calculated. We use a parametrization of $\pi\pi \to K\overline{K}$ from Ref. [14], which is based on the calculations [13]

$$\sigma_{\pi\pi\to K\overline{K}} = C\, 6.075 \left(1 - \frac{(2m_K)^2}{s}\right)^{0.76} (\text{mb}), \tag{2}$$

where the factor C is the combination of the Clebsch-Gordan coefficients for the respective isospin channels,

$$C = \sum_{I=0,1} |\langle i_1 i_2 m_1 m_2 | i_1 i_2 I M\rangle|^2 |\langle i_3 i_4 m_3 m_4 | i_3 i_4 I M\rangle|^2, \tag{3}$$

where i_k and m_k are the total isospin and the third isospin component of the particle k, respectively. Incoming and outgoing particles are enumerated by the pair of indices 1,2 and 3,4, respectively. For simplicity, we take the same cross section for $\rho\rho \to K\overline{K}$ and $\pi\rho \to K\overline{K}$ since the isospins of the incoming particles are the same; this is not the same result as that in Ref. [13]. For all other reactions with two nonstrange mesons in the incoming channel, we assume a constant value of 2 mb for the cross section. The back reactions are included, and their cross sections are calculated according to detailed balance.

By setting the cross sections constant we did not take into account the p-wave suppression of, e.g., $\pi\rho \to K\overline{K}$ near threshold. Due to the spin of the ρ meson, the strangeness production in that reaction is suppressed up to the threshold of $\pi\rho \to \overline{K}K^*$ and $\pi\rho \to \overline{K}^*K$. Including this suppression, however, has only a small effect on our results (see the discussions in Sec. IV and also Fig. 20).

Since the elementary reactions are not accessible experimentally, we test our choice of the cross sections by looking at the yields of kaons in heavy-ion collisions. Although this will give us only a rough estimate of our cross sections due to the presence of the baryon-baryon and the meson-baryon channels of the kaon production, there is no other way to get more reliable cross sections for meson-meson reactions.

B. Annihilation processes

Figure 1 (see dashed lines) shows[1] that we underestimate the strangeness production in the region just above the FRITIOF threshold ($\sqrt{s} > 2$ GeV). We see that directly above the threshold the cross section without the annihilation descends to almost zero.

This is due to the fact that the FRITIOF model is only capable of producing two excited hadrons, which fragment separately. Thus, it is not possible to describe Drell-Yan-like processes in which, e.g., a quark from an incoming baryon and an antiquark from an incoming meson annihilate (cf. Fig. 2). An example of such a process is $\pi N \to YK$, where Y stands for a hyperon.

For that reason, we have included the annihilation channel phenomenologically. In the case of a reaction of a baryon with a meson, we check if an annihilation between a quark and an antiquark is possible; we split each of the interacting hadrons into their constituents and check whether a quark and antiquark with the same flavor exist. If they exist, we annihilate the quark and antiquark with probability (4) and (5), neglecting any particles that might be created in this process. In order to make up for this neglect, we put all the energy and momentum of both incoming hadrons into the remaining quark content of the baryon and the meson. The fragmentation of this hadron is then done according to the Lund model. URQMD [15] interprets meson-baryon reactions in a similar way. RQMD [16] also includes baryon resonances with mass >2 GeV whose decay is described by the Lund model.

The probability for the annihilation is chosen such that we agree with experiment for the strangeness production in $\pi p \to$ strange particles (see solid lines in Fig. 1):

$$\text{Prob(annihilation)} = \max\left(0.85 - 0.17\frac{\sqrt{s}}{\text{GeV}}, 0\right). \tag{4}$$

[1] In Figs. 1, 3, 5, and 7, the statistical error bars are shown for the theoretical curves. They are calculated assuming a Poisson distribution, i.e., by dividing the plotted physical value by $\sqrt{N}$, where N is the total accumulated number of events which is used to construct the value. In all other figures, the statistical errors of theoretical results are either negligibly small or visible from the histogram representation.

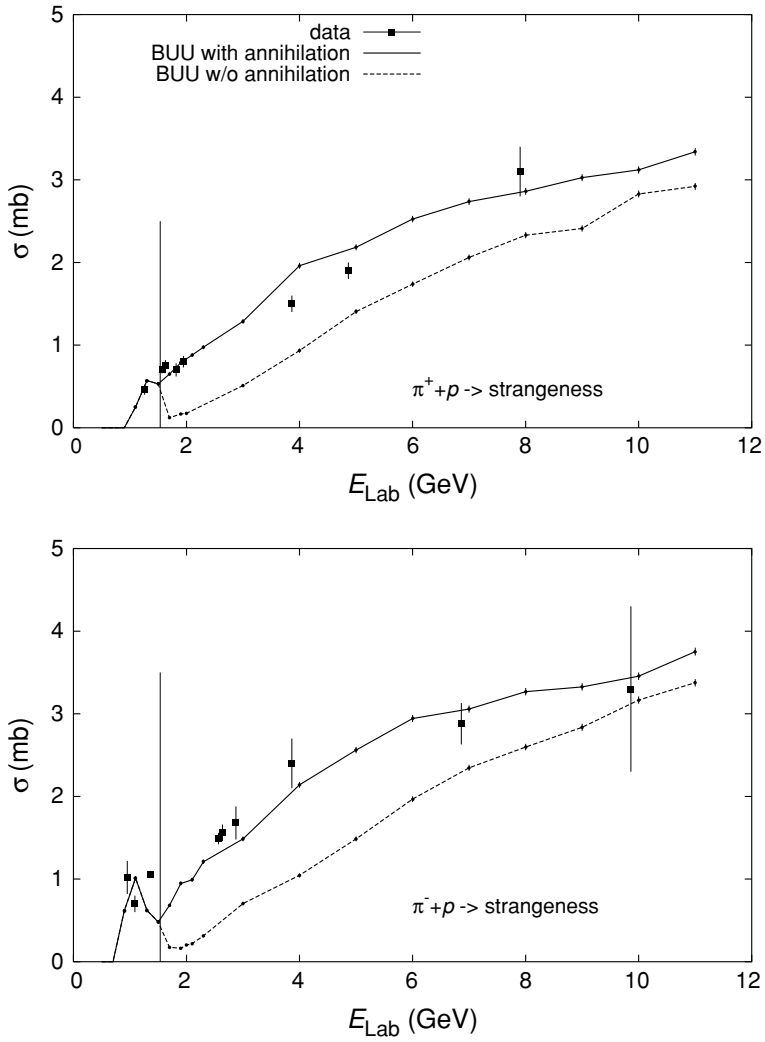

FIG. 1. The cross section of the strangeness production in $\pi^+ p$ collisions (upper panel) and $\pi^- p$ collisions (lower panel) as a function of beam energy in comparison to data from [39]. The vertical line corresponds to the threshold for the string model ($\sqrt{s} = 2\,\mathrm{GeV}$). Solid and dashed lines show results with and without $q\overline{q}$ annihilation channels (see Sec. II B), respectively. Error bars on calculations are statistical.

For the constant strangeness suppression factor $\gamma = 0.3$, the probability for the annihilation processes is readjusted:

$$\mathrm{Prob(annihilation)}_{\gamma=0.3} = \max\left(1.2 - 0.2\frac{\sqrt{s}}{\mathrm{GeV}}, 0\right). \qquad (5)$$

There are two main reasons for the increase of the strange particle production with inclusion of the annihilation. First, we include new channels, as discussed above. Another point is that the invariant energy per string decay is higher. If we have two strings instead of one, the two strings decay separately and therefore it will often occur that every string alone is below the threshold for strangeness production. By putting all the energy into one string, the invariant energy becomes higher and the production of strangeness more probable.

III. SYSTEM-SIZE DEPENDENCE

In order to clarify the reaction mechanisms in heavy-ion collisions, it is instructive, first, to understand the proton and light-ion induced reactions. For larger mass numbers of colliding nuclei, the effect of secondary hadron-hadron collisions becomes more and more important. These collisions drive the system toward thermal equilibrium and enhance the maximum baryon density reached in the collision process. Thus, by increasing the system size, we can also see how particle spectra evolve with increasing density and if our model within the standard parameters is able to reproduce the experimental measurements. In the discussion of numerical results, it is assumed, if the opposite is not stated explicitly, that the meson-meson cross sections and the

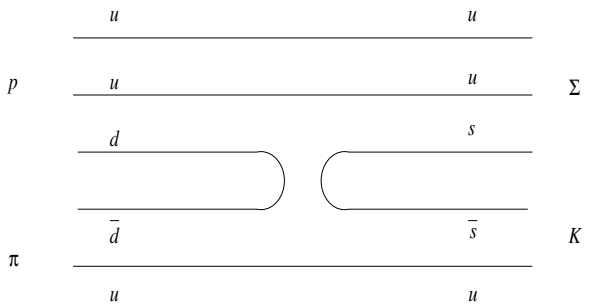

FIG. 2. Quark diagram for the process $\pi^+ p \to \Sigma^+ K^+$.

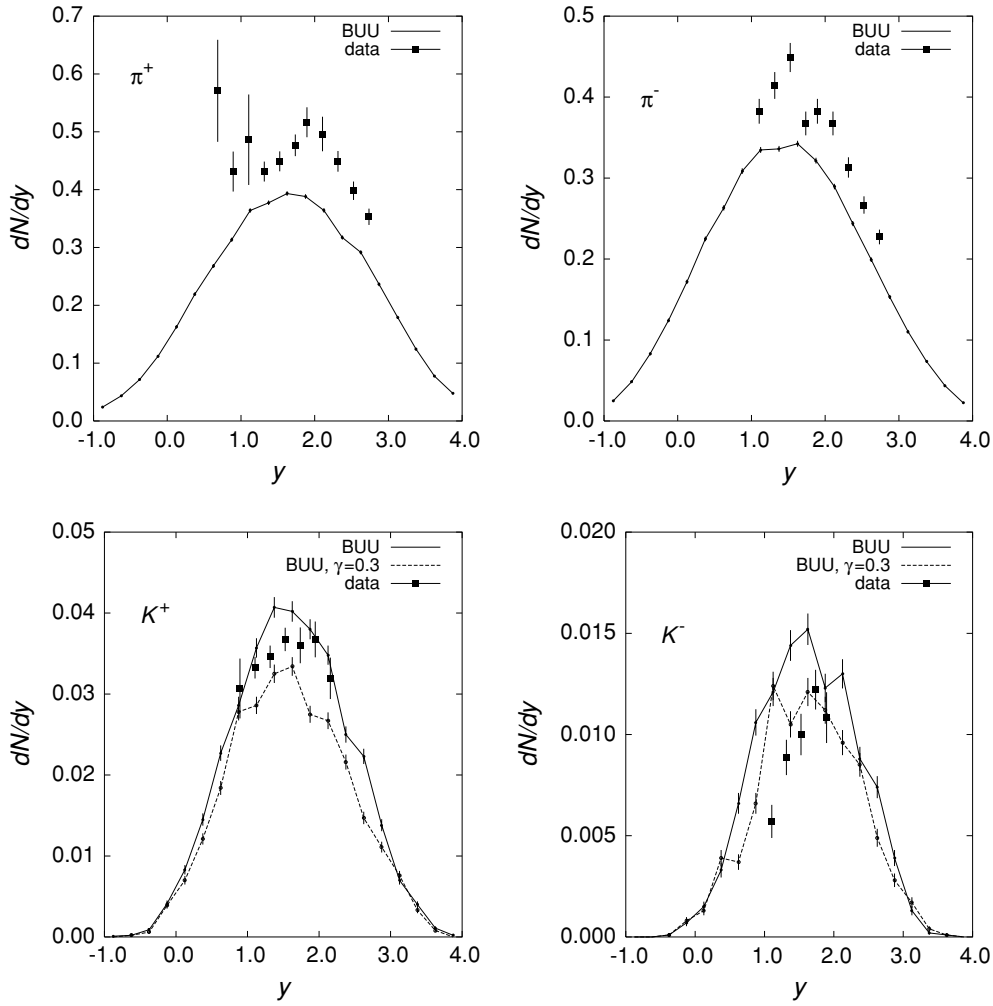

FIG. 3. Rapidity distributions of $\pi^{\pm}$ and $K^{\pm}$ for p+Be at 14.6 GeV/c in comparison to data from [17]. Solid and dashed lines show results with energy dependent [see Eq. (1)] and constant ($\gamma = 0.3$) strangeness suppression factors, respectively. Error bars on calculations are statistical.

$q\bar{q}$ annihilation are included, as described in the previous section.

First, we study the proton induced reactions p+Be and p+Au at a beam momentum of 14.6 GeV/c measured at BNL-AGS [17]. Figure 3 shows rapidity distributions of produced $\pi^{\pm}$ and $K^{\pm}$ for the p+Be system. In this case of a light target, the pions and kaons are produced mostly in the first-chance nucleon-nucleon (NN) collisions and have only a small probability of rescattering afterwards. Therefore, their rapidity distributions are centered near the NN center-of-mass (c.m.) rapidity $y_{NN} = y_{\rm beam}/2 = 1.72$. The pion yield is underestimated by ∼20%, whereas the kaon and antikaon yields are well described by BUU for the p+Be system.

According to Ref. [17], we have fitted the calculated transverse mass spectra with an exponential function

$$\frac{d^2\sigma}{2\pi m_\perp dm_\perp dy} = a \exp\{-m_\perp/T\} \qquad (6)$$

at various rapidities y. Figure 4 presents the inverse slope parameter T as a function of rapidity for π^+ and K^+ in the case of p+Be collisions. The pion inverse slope parameter is well reproduced by BUU except for the very forward and the very backward rapidities in the NN c.m. system. The calculated kaon inverse slope parameter overestimates the data by ∼20% at y_{NN}.

Figure 5 shows the rapidity distributions of $\pi^{\pm}$ and $K^{\pm}$ for the p+Au collisions. These distributions are shifted to smaller rapidities $y < y_{NN}$ with respect to the case of the p+Be reaction (Fig. 3) due to the contribution of the secondary NN and πN collisions to the meson production and rescattering of the produced mesons on the target nucleons. The K^- rapidity distribution is narrower and is shifted somewhat less than the K^+ distribution, since an antikaon is always produced together with a kaon, while a kaon can also be produced in association with a hyperon, which requires less c.m. energy [17]. Thus, the secondary NN and πN collisions contribute more to K^+ than to K^- production. BUU describes the experimental pion and kaon rapidity distributions within ∼20%. In Fig. 6, we

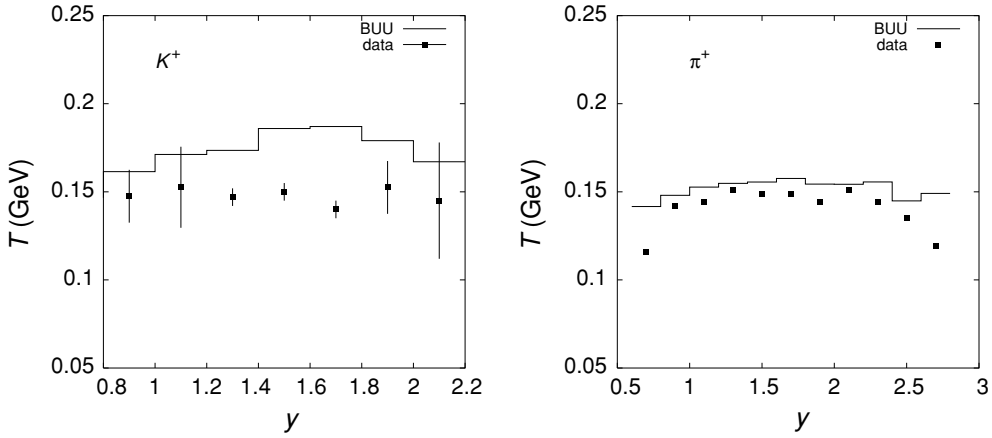

FIG. 4. Rapidity dependence of the inverse slope parameter T of the transverse mass spectra of π^+ and K^+ for p+Be at 14.6 GeV/c in comparison to data from [17].

present the rapidity dependence of the inverse slope parameter T of the K^+ and π^+ transverse mass spectra for the p+Au reaction. There is good agreement between BUU and the data except for the very forward rapidity in the π^+ case where we overpredict the experiment by ∼25%.

In agreement with the data, we observe little change in the value (∼150 MeV) of the inverse slope parameter for π^+ and K^+ with increasing target mass (cf. Figs. 4 and 6). The K^+ yield at $y = y_{NN}$ shows a factor of 2 enhancement, while the K^- yield at $y = y_{NN}$ stays practically unchanged both in BUU and in the data (cf. Figs. 3 and 5). We attribute this behavior to the stronger absorption of K^- in the heavier target. The experimental pion yield at $y = y_{NN}$ is the same for both systems, whereas in BUU we observe a slight

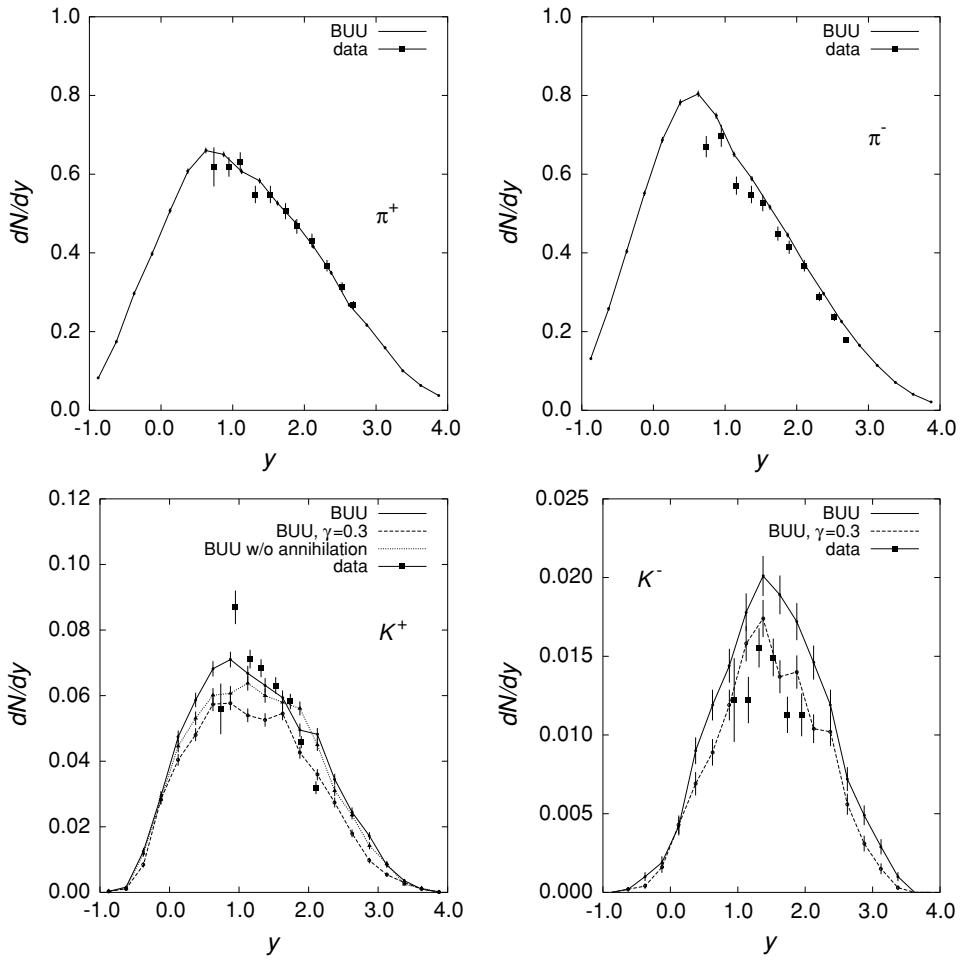

FIG. 5. Rapidity distributions of $\pi^\pm$ and $K^\pm$ for p+Au at 14.6 GeV/c in comparison to data from [17]. Solid and dashed lines show results with energy dependent [see Eq. (1)] and constant ($\gamma = 0.3$) strangeness suppression factors, respectively. The dotted line in the lower left panel shows a calculation without the $q\bar{q}$-annihilation channel in meson-baryon collisions. Error bars on calculations are statistical.

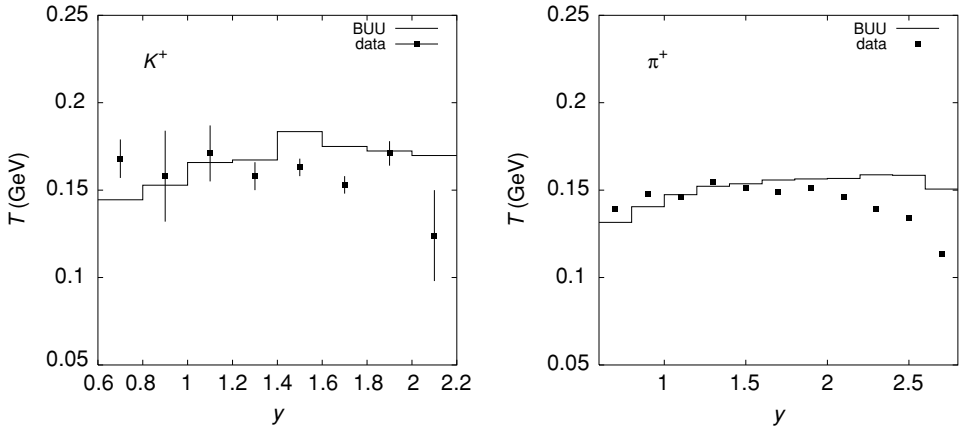

FIG. 6. Rapidity dependence of the inverse slope parameter T of the transverse mass spectra of π^+ and K^+ for p+Au at 14.6 GeV/c in comparison to data from [17].

enhancement of the pion yield at $y = y_{NN}$ with increasing target mass.

Next, we present results for Si+Au collisions at the beam momentum of 14.6A GeV/c, which were studied experimentally in Ref. [1]. This reaction has previously been studied theoretically in Refs. [16,18]. In Ref. [16], the RQMD model has been employed, which includes known nonstrange baryon resonances with $m < 2$ GeV. RQMD also describes the production of baryon resonances with $m > 2$ GeV in high-energy collisions; their decay is simulated by a string model. Shapes of the $\pi^{\pm}$ and $K^{\pm}$ transverse momentum spectra are quite well described by RQMD. No conclusions on the agreement of the absolute yields of the produced particles with data have been drawn in [16] due to the absolute normalization on the experimental π^+ spectra. However, ratios K^+/π^+ and K^-/π^- computed within RQMD agree well with data. In Ref. [18], a Relativistic Hadronic Cascade (ARC) model has been used; a pure hadronic scenario without string excitation was assumed. A good agreement between the ARC calculations and the E-802 data on proton $m_\perp$ spectra, and proton, π^+, and K^+ rapidity distributions was reached within the resonance model, i.e., when, e.g., a three-pion production channel in an NN collision is simulated as $NN \to \Delta\Delta\pi$ rather than directly as $NN \to NN\pi\pi\pi$. Inverse slope parameters of the $m_\perp$ spectra for protons and pions are well described by ARC but underestimated by ~20% for kaons.

We have considered only central collisions Si+Au corresponding to 7% of the inelastic cross section selected on multiplicity of charged particles [1]. In the theoretical calculations, we selected the central collisions in the same way. Figure 7 shows the calculated $\pi^{\pm}$ and $K^{\pm}$ rapidity distributions which were divided by the projectile mass (28) in order to be able to directly compare them with the rapidity distributions from the proton induced reactions.

By comparing the data points in Figs. 7 and 5, we see that the pion yields at $y = y_{NN}$ are, practically, the same in p+Au and Si+Au systems. This feature is not reproduced by BUU: there is an enhancement of the pion yield per projectile nucleon in the system Si+Au with respect to the p+Au system in our calculations. This may indicate a problem with pion production (or reabsorption) in the heavy system. The experimental $K^{\pm}$ yields per nucleon are higher in the Si+Au case than in the p+Au case, which is well reproduced by BUU.

In Fig. 8, we present the inverse slope parameters of the K^+ and π^+ transverse mass spectra. Despite the big error bars, plus systematic errors of ±10% which are not included in the error bars of the experimental data [1], we see that BUU underpredicts the inverse slope parameter for the K^+'s by about 25% and for the π^+'s by 15%. The calculated inverse slope parameter T stays practically constant within 150–160 MeV for all three systems p+Be, p+Au, and Si+Au for both the π^+'s and the K^+'s, whereas the experimental data show a higher $T \simeq 200$ MeV for K^+'s in the Si+Au system.

Studying strangeness production in more detail, we have also performed the BUU calculations using the constant energy independent strangeness suppression factor $\gamma = 0.3$ (dashed lines in Figs. 3, 5, and 7). The K^+ rapidity distributions favor the energy dependent strangeness suppression factor, while the K^- spectra are better described with $\gamma = 0.3$.

In order to demonstrate an effect of the $q\bar{q}$ annihilation on the K^+ production (see discussion in the previous section), we also show in Fig. 5 the results without the annihilation. In the p+Au system, the secondary πN and ρN collisions already play an important role. Thus, including the annihilation improves agreement with the data (cf. the solid and dotted lines in the lower left panel of Fig. 5).

The heaviest colliding system measured at AGS is Au+Au at the beam energies of 2–10.7A GeV [9,19,20]. Before discussing the beam energy dependence (see next section), we consider the centrality dependence of the pion and kaon production for Au+Au collisions at the top AGS energy of 10.7A GeV [9].

In Ref. [9], the collision centrality was determined using two criteria: (i) The energy deposited in the zero-degree calorimeter E_{ZCAL}, which gives an estimate of the projectile participant number N_{pp} as

$$N_{\mathrm{pp}} = 197 \times \left(1 - \frac{E_{\mathrm{ZCAL}}}{E_{\mathrm{beam}}^{\mathrm{kin}}}\right), \tag{7}$$

where $E_{\mathrm{beam}}^{\mathrm{kin}} = 2123$ GeV is the kinetic energy of the beam. The smaller E_{ZCAL} is, the larger the size of the participant zone, which selects geometrically more central events. (ii) The second criterion is the multiplicity of particles with velocity $\beta > 0.8$ in the New Multiplicity Array (NMA) $\mathrm{mult}_{\mathrm{NMA}}$. The velocity cut filters out the slow protons, whereas the produced

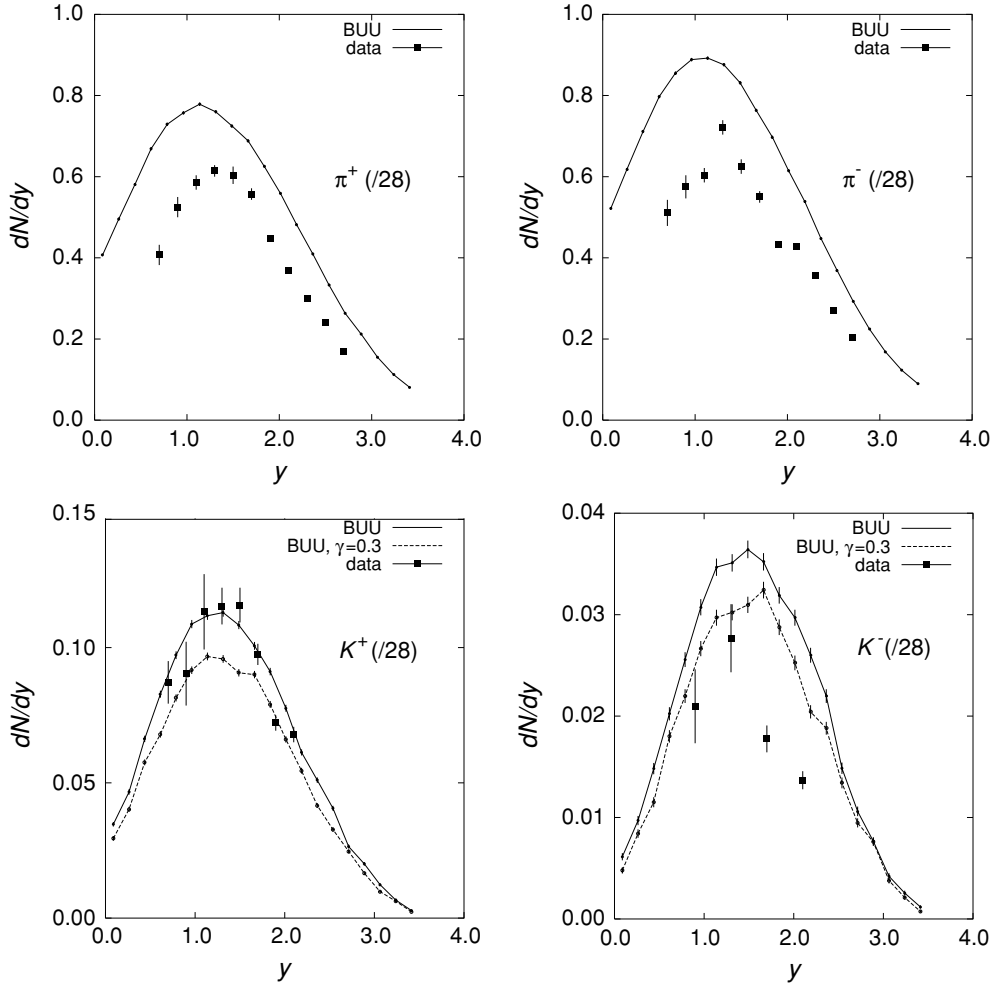

FIG. 7. Rapidity distributions of $\pi^{\pm}$ and $K^{\pm}$ for central collisions Si+Au at 14.6A GeV/c in comparison to data from [1]. Solid and dashed lines show results with energy dependent [see Eq. (1)] and constant ($\gamma = 0.3$) strangeness suppression factors, respectively. The spectra are divided by 28 in order to be able to compare them to proton-induced reactions. Error bars on calculations are statistical.

mesons (mostly pions) are accepted. Thus, the larger mult_{NMA} corresponds to the larger energy transfer from the longitudinal motion of colliding nuclei to the meson production. On average, events with a smaller impact parameter b have a larger mult_{NMA}. However, at fixed b the multiplicity mult_{NMA} fluctuates stochastically event-by-event depending on the amount of stopping of the counterstreaming nuclear matter in the interaction zone.

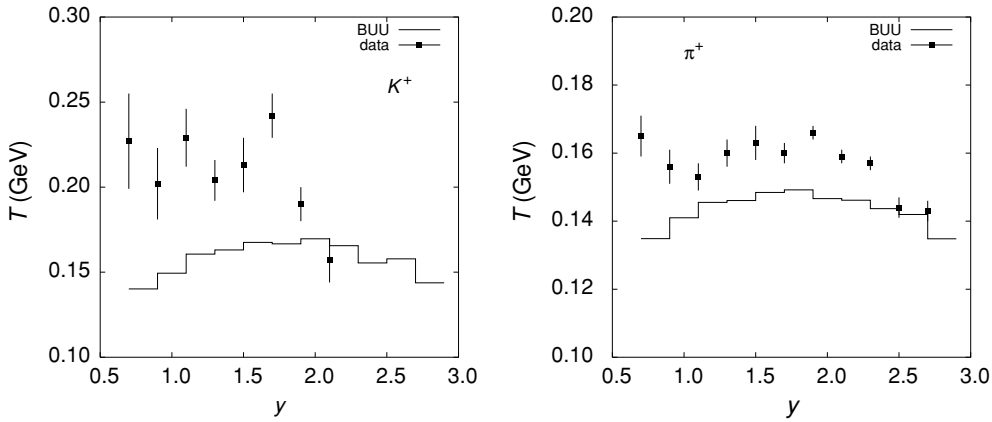

FIG. 8. Rapidity dependence of the inverse slope parameter T of the transverse mass spectra of π^+ and K^+ for Si+Au at 14.6A GeV/c in comparison to data from [1].

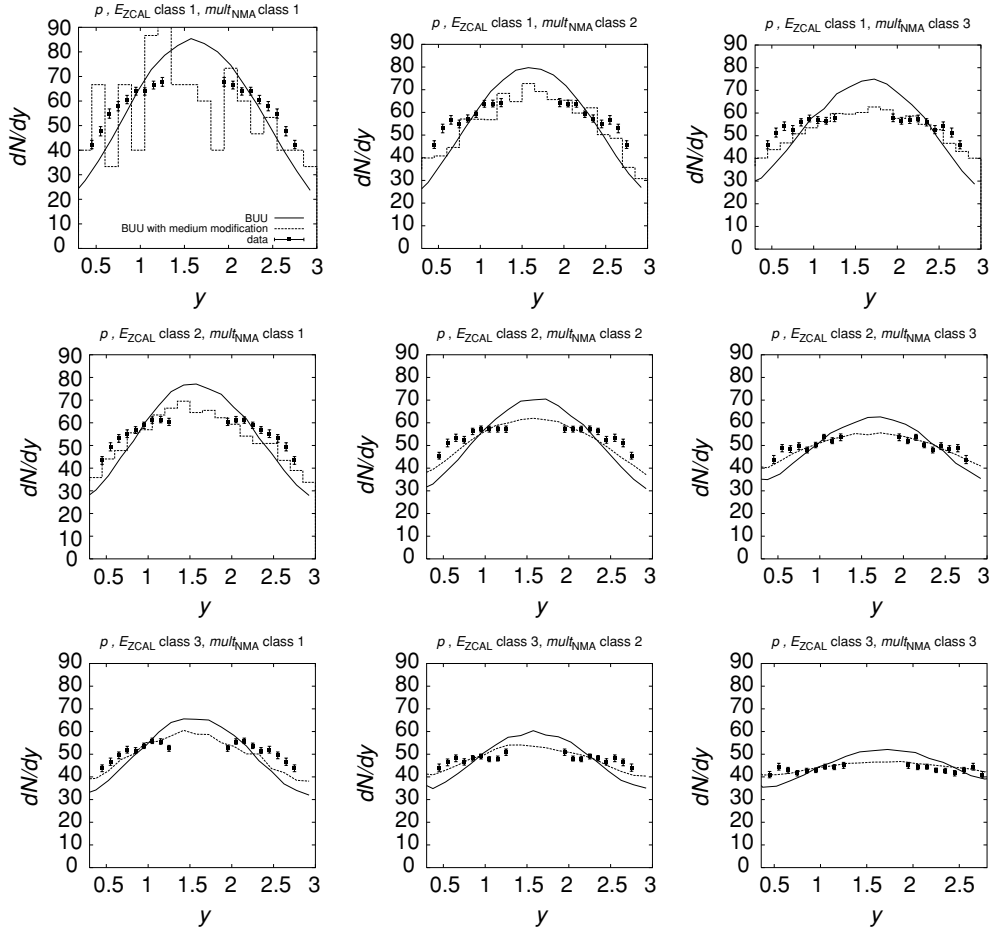

FIG. 9. Proton rapidity spectra from BUU events Au+Au at 10.7A GeV double selected on $\mathrm{mult_{NMA}}$ and E_{ZCAL} in comparison to data from [9]. The centrality decreases from the upper left corner to the lower right. The solid line shows the standard BUU calculation, whereas the dashed line is calculated with the medium modification described in Sec. V.

According to Ref. [9], we first divided BUU events, using E_{ZCAL}, into eight classes with increasing E_{ZCAL} (decreasing centrality) from the first to the eighth class (see Table II in [9]). Second, by modeling the NMA acceptance, we subdivided each of the first three E_{ZCAL} event classes into the three $\mathrm{mult_{NMA}}$ classes with decreasing $\mathrm{mult_{NMA}}$ (decreasing centrality) from the first to the third multiplicity class (see Table III in [9]).

Figure 9 shows the proton rapidity distributions for various combinations of E_{ZCAL} and $\mathrm{mult_{NMA}}$ event classes. We see that in each case BUU overestimates stopping. Agreement with experiment can be improved by taking into account the in-medium corrections to the FRITIOF model (see Sec. V).

Figures 10 and 11 show the rapidity spectra of pions and kaons for different event classes selected by applying the E_{ZCAL} cut only. The K^+ rapidity spectra are very well described for all E_{ZCAL} classes. For the π^+ rapidity spectra, we see deviations from the data: In the most central collisions, there are excessive pions in BUU produced mainly at midrapidity. With decreasing centrality, the deviation from the data disappears gradually, and in the most peripheral collisions there is even an underprediction of the pion multiplicity by BUU. These results are consistent with Figs. 3, 5, and 7, where one can also observe a tendency to overpredict pion production with increasing size of the participant zone.

Figures 12 and 13 show transverse mass spectra of the π^+'s and K^+'s for the central collisions of Au+Au at 10.7A GeV. The spectra are shown for various rapidities starting from the backward rapidity in the c.m. frame (upper line) to the midrapidity (lower line). The shapes of the π^+ spectra are well described by standard BUU; however, the π^+ yields are slightly overpredicted at small $m_\perp$ (see also the upper left panel in Fig. 10). The agreement of BUU with the K^+ spectra is much poorer. The low $m_\perp$ part of the K^+ spectra is, typically, overestimated by BUU, whereas the high $m_\perp$ part of the spectra is underestimated by our calculations. Thus, BUU underestimates the inverse slope parameter of the K^+ transverse mass spectra, while the K^+ yield is well described (cf. the upper left panel in Fig. 11). This problem was pointed out previously in Ref. [21].

Figure 14 shows a fiducial yield of K^+ and π^+ divided by the projectile participant number N_{pp} as a function of N_{pp}. The fiducial yield is defined as [9]

$$\text{fiducial yield} = \sum_{0.6<y<1.3} \frac{dN}{dy} dy, \tag{8}$$

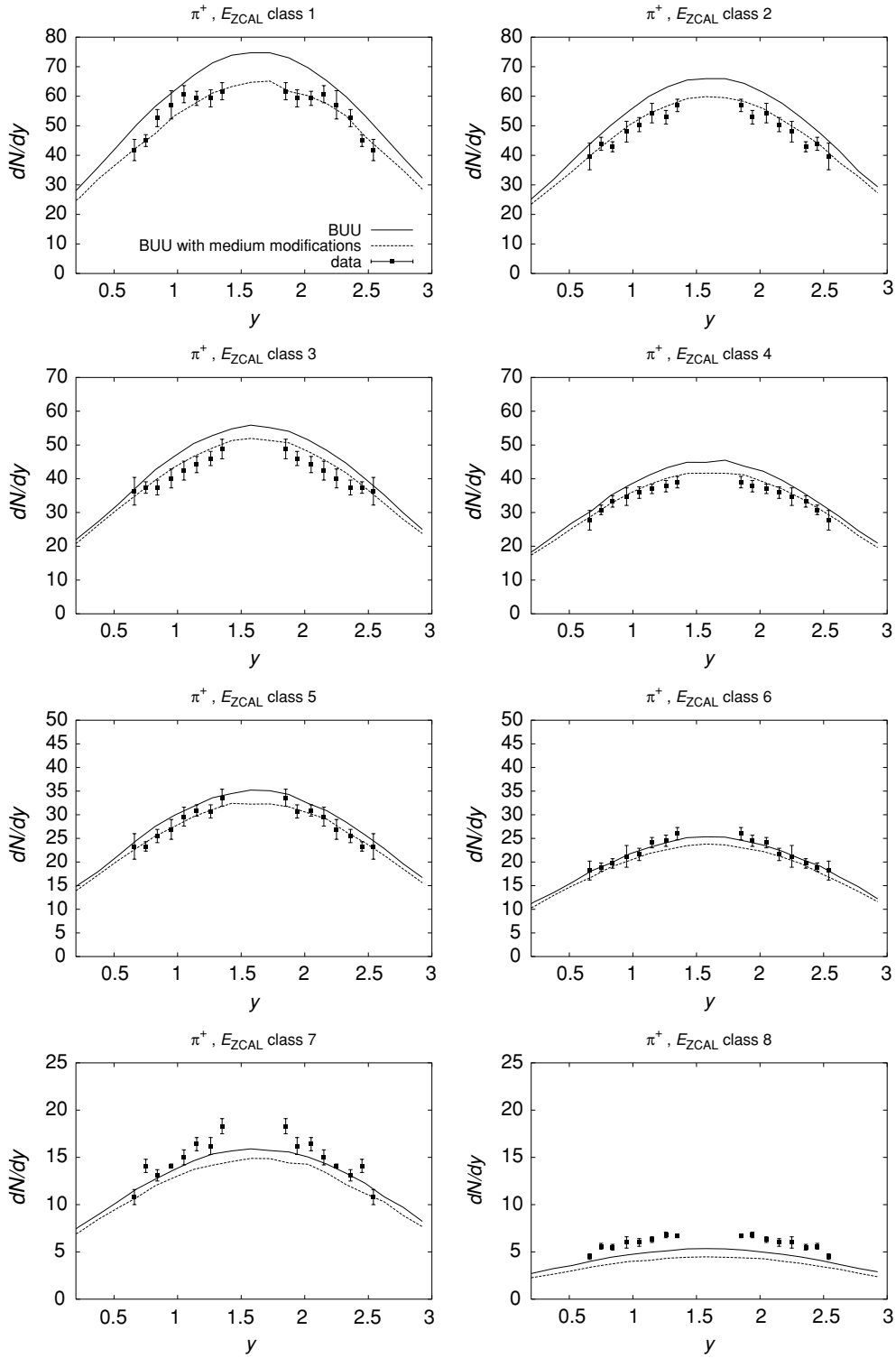

FIG. 10. Rapidity spectra of π^+ from BUU events Au+Au at 10.7A GeV selected by the zero-degree energy in comparison to data from [9]. The centrality decreases from the upper left corner to the lower right. The solid line shows the standard BUU calculation, whereas the dashed line is calculated with the medium modification described in Sec. V.

where the dN/dy are the rapidity distributions selected by the zero-degree energy. The K^+ fiducial yield, as expected, agrees quite well with the data except for a slight underprediction at peripheral collisions. The π^+ fiducial yield increases with $N_{\rm pp}$ faster than the data do. In the absence of secondary NN collisions, the fiducial yields divided by $N_{\rm pp}$ would be constant.

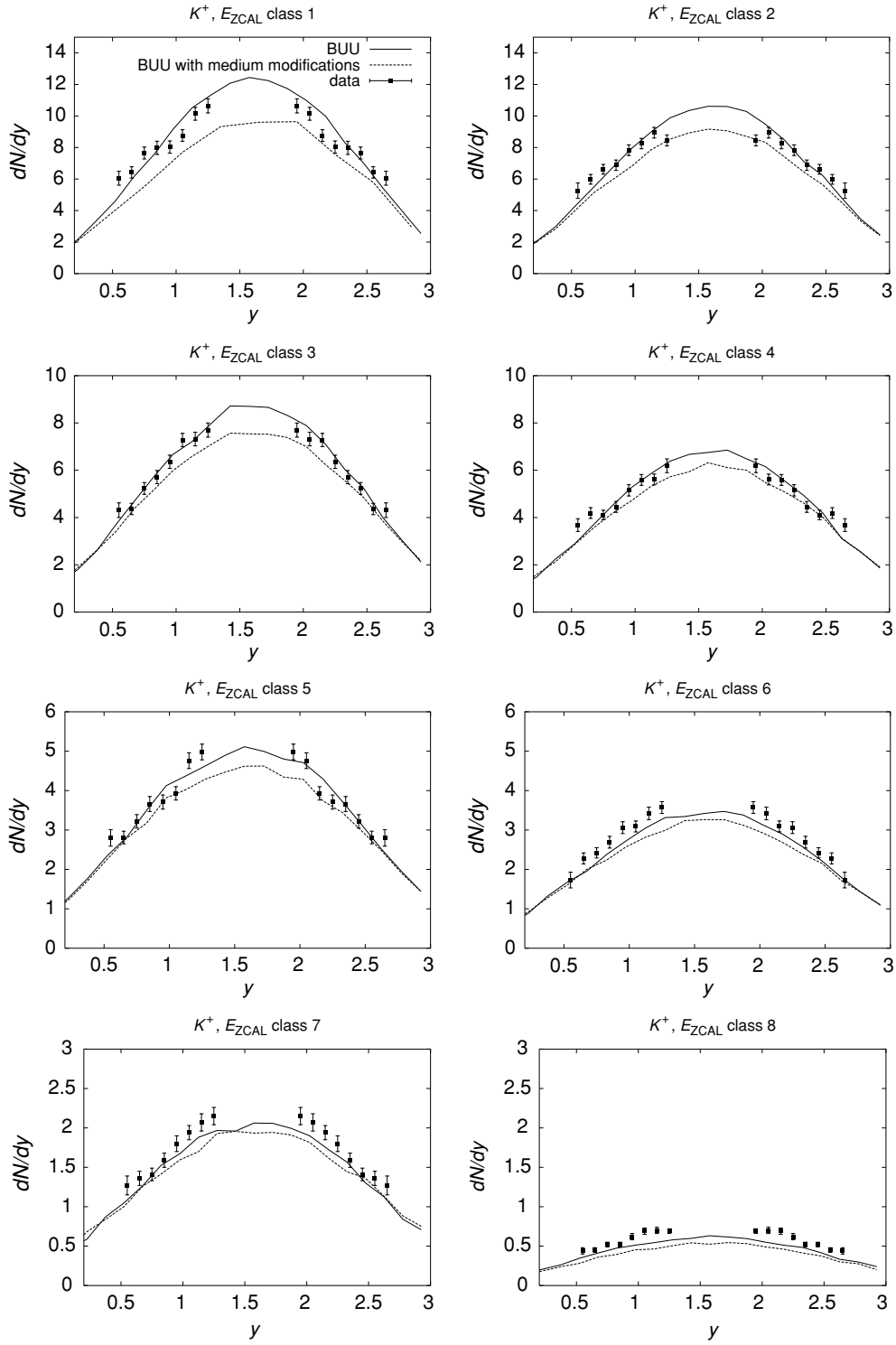

FIG. 11. Rapidity spectra of K^+ from BUU events Au+Au at 10.7A GeV selected by the zero-degree energy in comparison to data from [9]. The centrality decreases from the upper left corner to the lower right. The solid line shows the standard BUU calculation, whereas the dashed line is calculated with the medium modification described in Sec. V.

IV. EXCITATION FUNCTIONS

In this section, we show the excitation functions of pions, kaons, and Λ and Σ hyperons from central Au+Au and Pb+Pb collisions in comparison to data, two other transport models HSD and UrQMD [6], and the statistical model [22]. The calculations performed with the transport models have all been done in the cascade mode, which makes the comparison easier. We selected the data sets for the Au+Au system at 1.96, 4.00, 5.93, 7.94, and 10.7A GeV [19,20], with 5% of the most

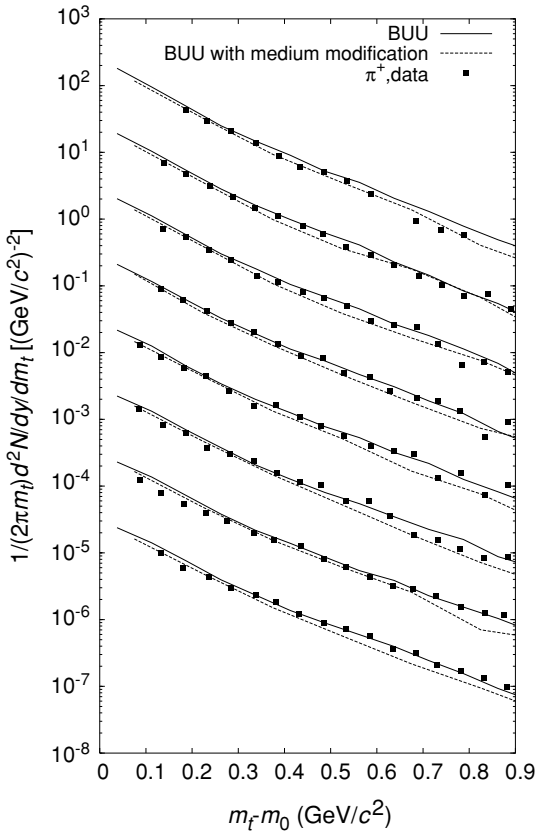

FIG. 12. Transverse mass spectra for π^+ from Au+Au collisions at 10.7A GeV for different slices of rapidity from the most central events selected by E_{ZCAL}. The rapidity slices range from 0.6–0.7 for the uppermost line to 1.3–1.4 for the lowermost line with a step of 0.1. The spectra are multiplied by powers of 10: $10^0, 10^{-1}, \ldots, 10^{-7}$ from the uppermost to the lowermost line. Data are from [9].

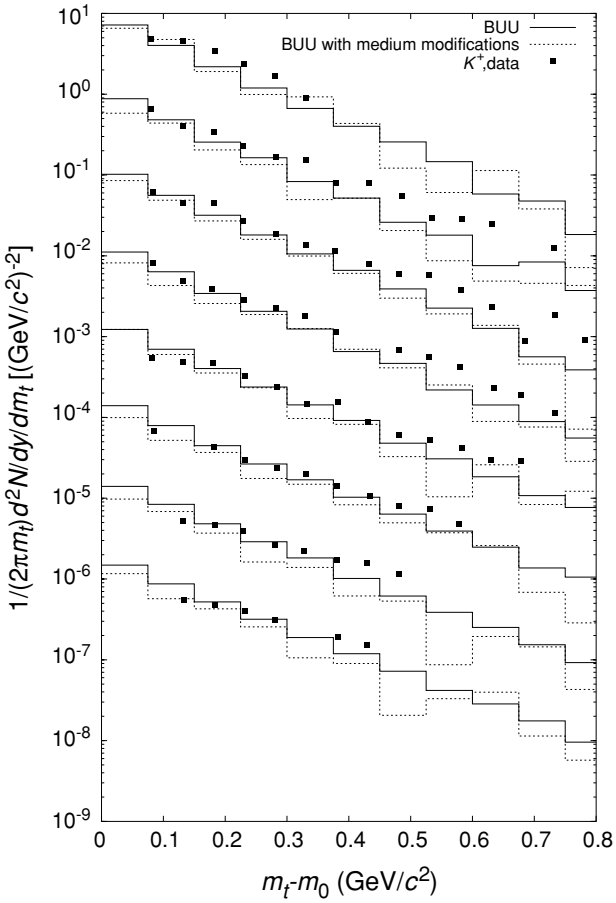

FIG. 13. Transverse mass spectra for K^+ from Au+Au collisions at 10.7A GeV for different slices of rapidity from the most central events selected by E_{ZCAL}. The rapidity slices range from 0.5–0.6 for the uppermost line to 1.2–1.3 for the lowermost line. The spectra are multiplied by powers of 10: $10^0, 10^{-1}, \ldots, 10^{-7}$ from the uppermost to the lowermost line. Data are from [9].

central events, and for the Pb+Pb system at 30 and 40A GeV [3,23], with 7% of the most central events. In the theoretical calculations, we used a sharp impact parameter cutoff at 3.5 fm for AGS energies and at 4 fm for SPS energies. The influence of the centrality selection was tested at 10.7A GeV by comparing calculations with a sharp cutoff to calculations done by employing the centrality criteria described in Sec. III. No

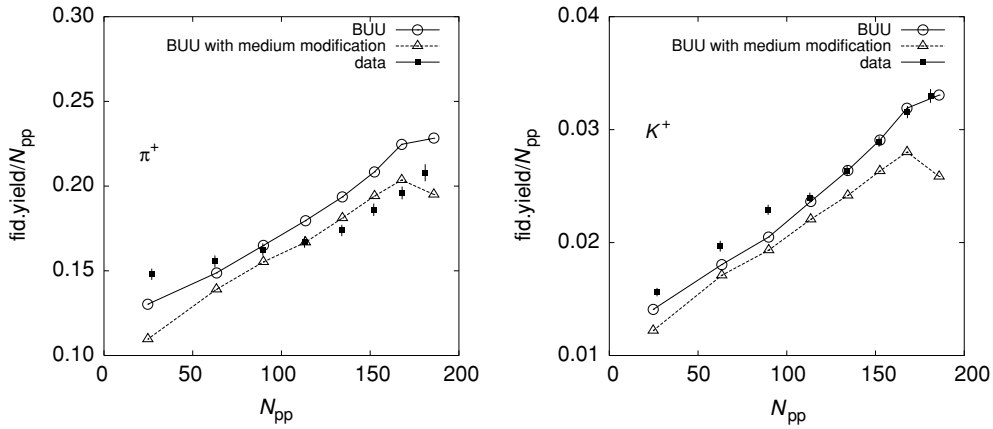

FIG. 14. Fiducial yields of π^+ and K^+ divided by the number of projectile participants N_{pp} as functions of N_{pp} from Au+Au collisions at 10.7A GeV in comparison to data from [9].

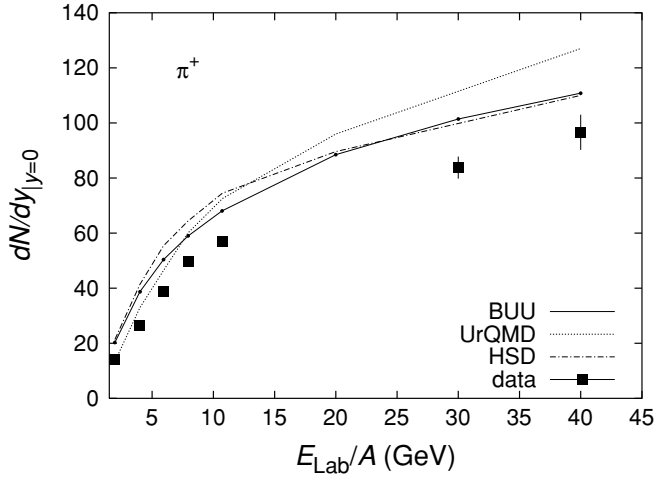

FIG. 15. Midrapidity yields for π^+ as a function of energy in comparison to results of HSD, results of UrQMD, and data from [3,19,23].

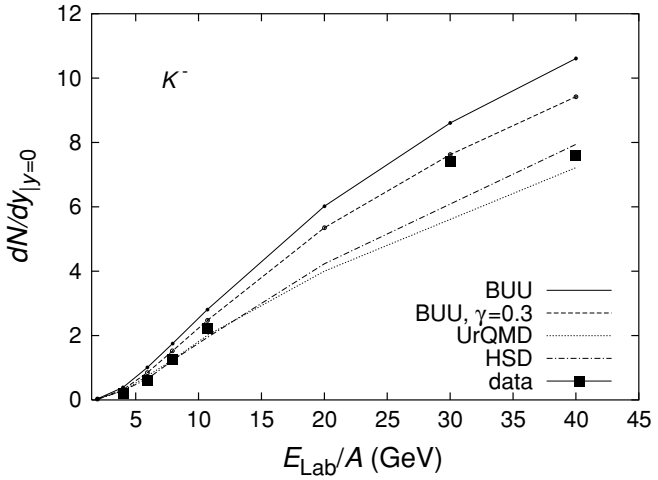

FIG. 17. Midrapidity yields for K^- as a function of energy in comparison to results of HSD, results of UrQMD, and data from [3,20,23].

deviations were seen in the observables, which are presented in the following.

Figure 15 shows the midrapidity yield of positive pions as a function of the beam energy. We see that all three models overpredict the pion yield in the considered beam energy range (2–40A GeV). Our model (solid line) overpredicts the π^+ midrapidity yield by $\sim$10% at 40A GeV to $\sim$50% at 2A GeV. However, the shape of the experimental excitation function dN/dy vs. $E_{\rm Lab}$ for π^+ is remarkably well described by BUU. The HSD model (dot-dashed line) produces the π^+ yields close to the BUU results excepting the points at 6, 8, and 10.7A GeV, where HSD has $\sim$10% more pions than BUU. The UrQMD model (dotted line) agrees well with the pion data at the smallest energy of 2A GeV, but the pion yield grows too fast with energy within UrQMD producing a discrepancy of $\sim$30% with data at the highest considered energy of 40A GeV.

Figures 16, 17, and 18 show the midrapidity yields of K^+, K^-, and $(\Lambda + \Sigma^0)$, respectively, as functions of the beam energy. BUU quite well describes the K^+ midrapidity yield excepting the points at 4 and 6A GeV, where BUU overestimates the data by 30–50%.

The K^- midrapidity yield and $(\Lambda + \Sigma^0)$ midrapidity yield at $E_{\rm Lab} < 40A$ GeV are overestimated by BUU. Using the constant strangeness suppression factor $\gamma = 0.3$ (dashed lines) reduces the yields of K^+, K^-, and hyperons. This leads to a better description of the K^- yields, while in the cases of K^+ and $(\Lambda + \Sigma^0)$ it is hard to judge which strangeness suppression factor works better. In Figs. 16 and 18, we see that up to about 10A GeV, the K^+ and hyperon yields are better described with $\gamma = 0.3$. Above that energy, however, the energy dependent suppression factor works better. For the antikaons, the strangeness exchange processes $\overline{K}N \leftrightarrow \pi Y$ are

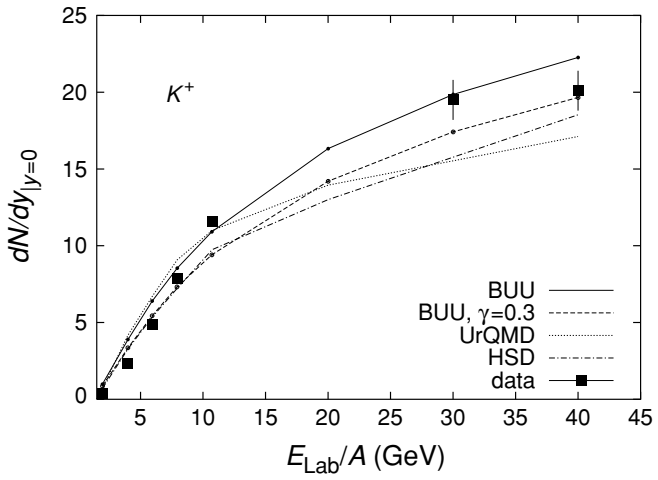

FIG. 16. Midrapidity yields for K^+ as a function of energy in comparison to results of HSD, results of UrQMD, and data from [3,19,23].

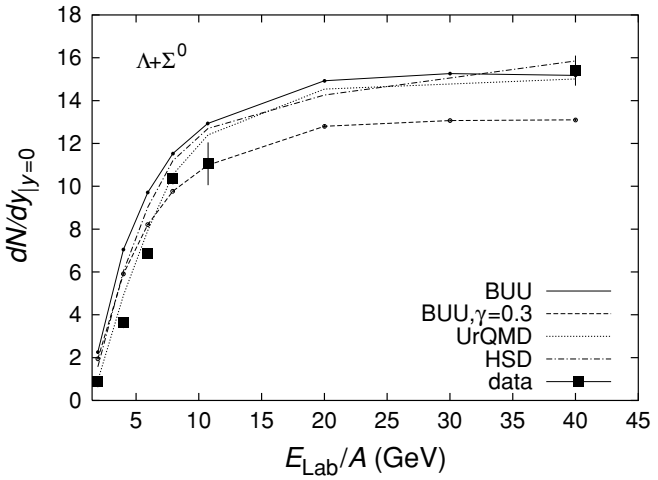

FIG. 18. Midrapidity yields for $\Lambda + \Sigma_0$ as a function of energy in comparison to results of HSD, results of UrQMD, and data from [40–44].

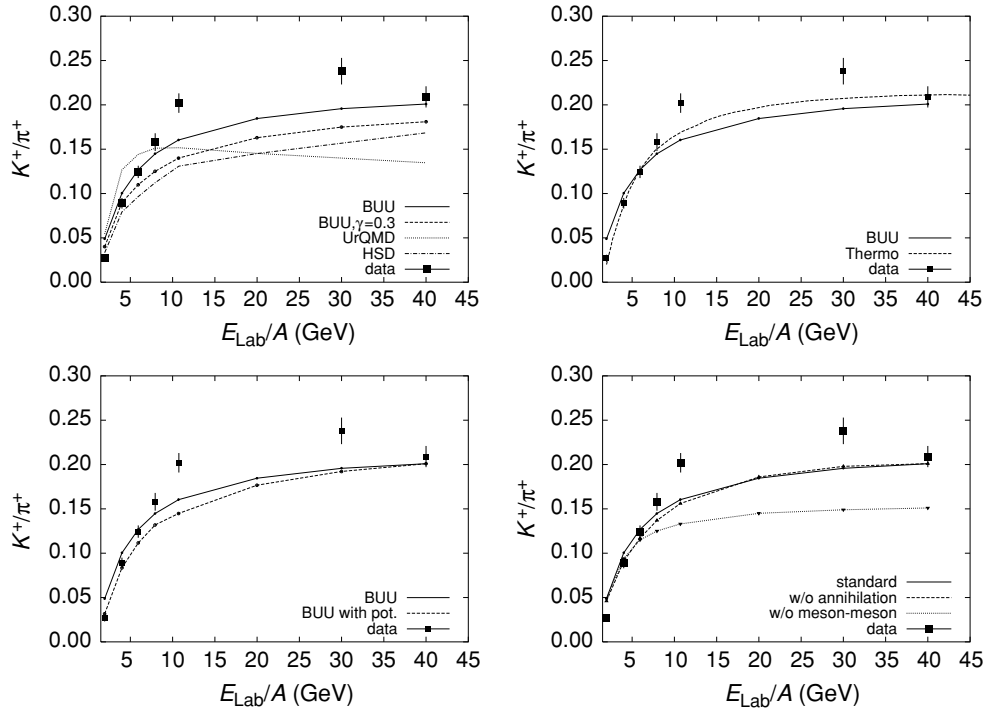

FIG. 19. K^+/π^+ ratio at midrapidity as a function of the beam energy. Upper left panel: comparison of the BUU results with the results of the UrQMD and HSD models [6]. Upper right panel: comparison between BUU and the statistical model [22]. Lower left panel: comparison of standard BUU (cascade mode) and BUU with nuclear mean field potential. Lower right panel: comparison of the standard BUU calculation with the calculations without $q\overline{q}$ annihilation and without meson-meson collisions. The data are from [3,19,23].

important due to the strong in-medium modifications [24], which are not taken into account in our study.

The HSD results on the K^+ production are close to our calculation with $\gamma = 0.3$. The UrQMD model gives the K^+ yield at lower energies similar to our standard calculation, whereas at higher energies UrQMD produces substantially fewer kaons. The K^- yield is rather well described by both models, HSD and UrQMD, except for the point at 30A GeV. At lower energies, the $(\Lambda + \Sigma^0)$ yields calculated within HSD and UrQMD are somewhat closer to the data than our standard calculation. At higher energies, the HSD, UrQMD, and our standard calculation give very close results for the $(\Lambda + \Sigma^0)$ yield.

Figure 19 shows the ratio of midrapidity yields of K^+ and π^+ as a function of the beam energy. In the upper left panel of Fig. 19 we see that neither BUU nor HSD and UrQMD describe the ratio K^+/π^+ in the whole beam energy region. At the lowest beam energy of 2A GeV, BUU and UrQMD overpredict the ratio by a factor of 2, whereas HSD agrees with the data. Between 4 and 8A GeV, BUU is quite close to the data. However, the K^+/π^+ ratio excitation function levels off too early in BUU, and as a consequence, we underestimate the ratio by ∼25% between 10 and 30A GeV. The HSD results on the ratio K^+/π^+ have a similar beam energy dependence, but the value of the ratio is smaller by ∼20%, which is close to our calculation with $\gamma = 0.3$. UrQMD produces a larger slope at lower energies, overestimating the ratio at $E_{\rm Lab} < 8A$ GeV, but at higher energies the slope gets negative, which causes a strong discrepancy with data in the SPS energy regime. Overall, we observe that BUU has the best agreement with data on the K^+/π^+ ratio in the considered energy regime. At beam energies of 4–6A GeV, however, this comes about due to cancellation of the overestimation of the pion and kaon yields.

Figure 20 shows the ratio of the midrapidity yields K^-/K^+ vs. the beam energy. The BUU calculations with the energy dependent strangeness suppression factor and our "standard"

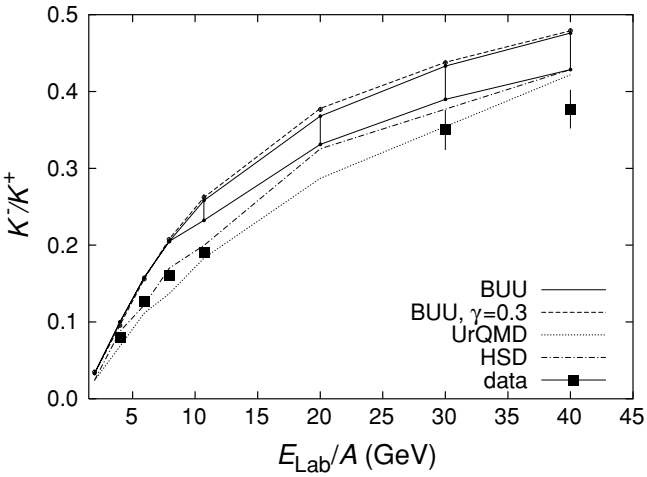

FIG. 20. The K^-/K^+ ratio at midrapidity as a function of energy in comparison to results of HSD, results of UrQMD, and data from [3,20,23]. The error band on the BUU results indicates the uncertainty in the meson-meson channels (see discussions in Secs. II A and IV).

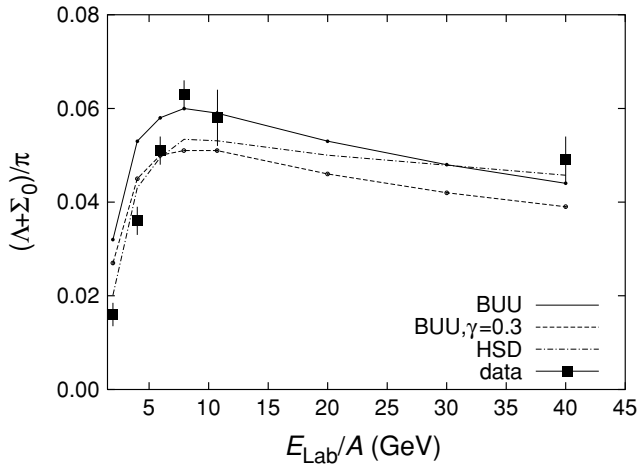

FIG. 21. The $(\Lambda + \Sigma^0)/\pi$ ratio at midrapidity, where $\pi = 1.5(\pi^+ + \pi^-)$, as a function of energy in comparison to data from [40–44].

meson-meson cross sections are shown as the upper boundary of the error band. In order to estimate an effect of the p-wave suppression on the $\pi\rho \to K\overline{K}$ and $\pi\omega \to K\overline{K}$ cross sections (see Sec. II A), we also performed a calculation by putting the cross section equal to zero below the $K^*\overline{K}$ production threshold, which is shown by the lower boundary of the error band in Fig. 20. Thus, the p-wave suppression could reduce the K^- multiplicity by about 10%. The K^+ multiplicity is reduced less than 5% by this effect, since the fraction of K^+ coming from meson-meson collisions is less than the fraction of K^- coming from meson-meson reactions. (For this reason, our results on the K^+/π^+ ratio, shown in Fig. 19, are practically untouched by the p-wave suppression effect.)

Overall, we see that BUU overestimates the K^-/K^+ ratio independent of the strangeness suppression factor. This result is expected from the results shown in Figs. 16 and 17, where we see that the K^+ yield is rather well described by BUU, while the K^- yield is overestimated substantially. Since the choice $\gamma = 0.3$ reduces both K^+ and K^- yields, the ratio K^-/K^+ is practically independent of the strangeness suppression factor. The HSD and UrQMD models describe the experimental K^-/K^+ ratio quite well. This can be also traced back to Figs. 16 and 17.

Figure 21 shows the ratio of the midrapidity yields $(\Lambda + \Sigma^0)/\pi$ vs. the beam energy. This ratio has a peak near $E_{\rm Lab} = 8A$ GeV, which is reproduced by the BUU and HSD models. As far as the absolute values of this ratio are concerned, at small energies $E_{\rm Lab} < 10A$ GeV, we would like to note again that both pion and hyperon yields are overestimated by standard BUU (see Figs. 15 and 18). Thus, the agreement of standard BUU with data on $(\Lambda + \Sigma^0)/\pi$ at 8 and 10.7A GeV is again a result of a mutual cancellation of the $(\Lambda + \Sigma^0)$ and π excesses. The choice of $\gamma = 0.3$, which describes the $(\Lambda + \Sigma^0)$ midrapidity yield at small energies better (cf. Fig. 18), leads to the underestimation of the $(\Lambda + \Sigma^0)/\pi$ ratio at the peak due to the overestimation of the pion yield.

All calculations discussed above were performed in the cascade mode. There is an option in our BUU model, which switches on a nuclear mean field potential. The nuclear mean field potential is necessary, in particular, for a description of the experimental data on collective in-plane and out-of-plane proton and neutron flows [25] at 0.15–2A GeV. At higher energies, however, the parametrization of the momentum dependent interaction used in [25] leads to a too repulsive in-plane flow (see also Ref. [26]). Nevertheless, in order to estimate the mean field effect on pion and kaon production, we have also done the calculation with the mean field potential (incompressibility $K = 215$ MeV, soft momentum dependent mean field SM). The lower left panel of Fig. 19 shows the results of this calculation (dashed line) in comparison with our standard calculation in the cascade mode (solid line) and with experimental data. We see that at $E_{\rm Lab} < 40A$ GeV, the ratio K^+/π^+ is reduced due to the mean field potential, since the pion yield is relatively insensitive to the nuclear mean field, whereas the kaon yield is reduced. Indeed, a part of the kinetic energy of the counterstreaming nucleon flows transforms now to the potential energy. This reduces, generally, particle production. However, kaon production is closer to its threshold than pion production. Therefore, kaons are more strongly influenced by the mean field potential than pions.

As we described in Sec. II, the meson-meson collisions and the $q\bar{q}$-annihilation channel for the meson-baryon collisions are implemented in our BUU model. The lower right panel of Fig. 19 shows an effect of these implementations on the K^+/π^+ midrapidity ratio. The result of our standard calculation, including both the meson-meson collisions and the $q\bar{q}$ annihilation, is shown by the solid line in Fig. 19. The dotted and dashed lines represent the calculations without the meson-meson collisions but with annihilation and without the annihilation but with the meson-meson collisions, respectively. The meson-meson collisions strongly enhance the K^+/π^+ ratio above 6A GeV due to the increased $K\bar{K}$ production. An effect of the $q\bar{q}$-annihilation channel is less pronounced: only a slight enhancement of the K^+/π^+ ratio is visible at $5-10A$ GeV.

The upper right panel of Fig. 19 compares the BUU and the statistical model [22] calculations for the K^+/π^+ ratio at midrapidity. Since we use a string model, which produces a multiparticle final state for the two colliding particles, the thermal equilibrium would be reached only if we also included the corresponding back reactions (cf. Ref. [27]). However, these are beyond the scope of the present work. Nevertheless, there is surprisingly good agreement between BUU and the statistical model. The statistical model is closer to the data, but it is also unable to describe the data points at 10 and 30A GeV.

Finally, in Fig. 22 we show the inverse slope parameter T of the K^+ transverse mass spectra vs. the laboratory energy. At the energies 2, 4, 6, and 8A GeV, the inverse slope parameter was obtained by fitting the exponential function (6) to the $m_\perp$ spectrum of kaons in the rapidity range $|(y - y_{NN})/y_{NN}| < 0.25$ [20]. At 10.7A GeV, the rapidity range was $|(y - y_{NN})/y_{NN}| < 0.125$ [20]. At the SPS energies of 30 and 40A GeV, the rapidity range was taken as $|y - y_{NN}| < 0.1$ [3,23]. Our model underestimates the inverse slope parameter by 30–40% (see also Fig. 13). A similar problem was reported

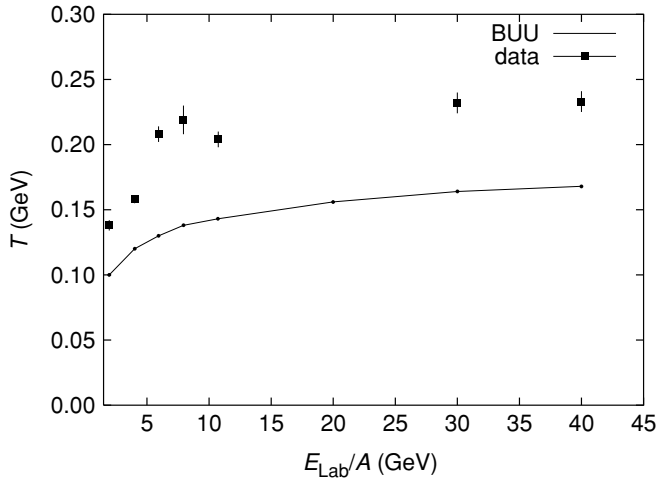

FIG. 22. Inverse slope parameter T for K^+ as a function of energy in comparison to data from [3,20,23].

before in Refs. [21,28] and ascribed to the lack of pressure due to missed nonhadronic degrees of freedom in the transport models. We speculate here that the inclusion of multibaryon collisions would also tend to make the spectrum harder. The probability for such processes naturally increases with a high power of baryon density.

In order to see an origin of the produced kaons, we performed a channel decomposition of the $\bar{s}$-quark production for the central Au+Au collisions at 4, 10.7, and 20A GeV. Figure 23 shows the number of the produced $\bar{s}$ quarks vs. time for four different channels: (i) the baryon-baryon channel at high energies ($\sqrt{s} > 2.6$ GeV) or, in other words, the baryon-baryon reactions simulated by the FRITIOF string model (solid line), (ii) baryon-meson collisions at $\sqrt{s} > 2$ GeV simulated by the string model (dashed line), (iii) baryon-meson collisions at $\sqrt{s} < 2$ GeV, i.e., below the string model threshold (dash-dotted line), and (iv) meson-meson collisions (dotted line). The low energy ($\sqrt{s} < 2.6$ GeV) baryon-baryon collisions do not contribute to the $\bar{s}$ production significantly at the considered beam energies. Thus, this channel is not shown in Fig. 23. We counted only the creation of the $\bar{s}$ quark, and we did not consider reactions or decays, as, e.g., $K^* \to K\pi$ where the $\bar{s}$ quark is only shifted from a K^* to a K.

The baryon-baryon-string channel plays the dominant role in the whole beam energy region. This channel includes mainly the first-chance NN collisions between the projectile and the target nucleons. The meson-meson channel is not important at 4A GeV, but its role grows quickly with energy, and at 20A GeV it already includes 25% of the produced $\bar{s}$ quarks. A relative contribution of the baryon-meson-string channel also increases with energy, while the low-energy baryon-meson collision relative contribution always stays very small and decreases with energy.

The time evolution of the $\bar{s}$-quark production can be better understood if one also looks at the central density time evolution shown in Fig. 24 for the central Au+Au collision at 10.7A GeV. The central density reaches its maximum value $\sim 4.5\rho_0$ at $t \simeq 10.5$ fm/c and stays above $3\rho_0$ in the time

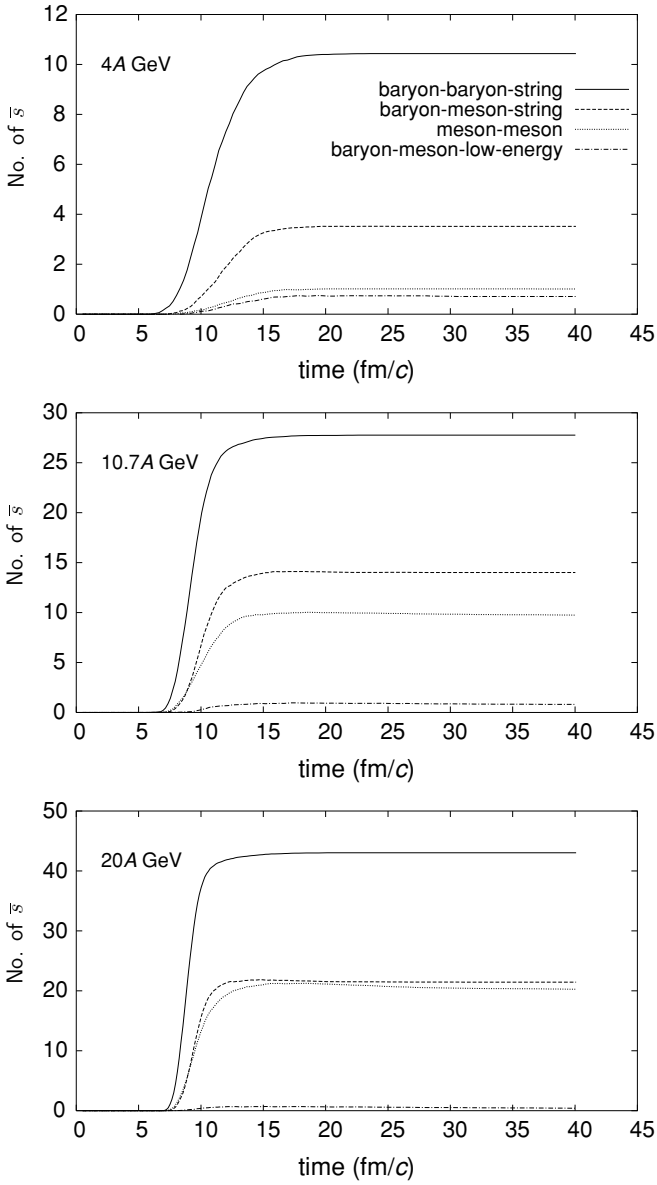

FIG. 23. Contribution of different channels to strangeness production in Au+Au collisions with $b = 1$ fm at 4A GeV (upper panel), 10.7A GeV (middle panel), and 20A GeV (lower panel).

interval $t = 7.5$–14 fm/c, where the $\bar{s}$-quark production takes place. Here, $\rho_0 = 0.16$ fm^{-3} is the nuclear saturation density. Thus, strangeness is produced during the high-density stage of a heavy-ion collision. It is evident also from Fig. 23 that the $\bar{s}$-quark production from the meson-meson and the baryon-meson channels, which contain the secondary collisions, starts later than that from the baryon-baryon channel.

V. IN-MEDIUM MODIFICATION OF THE FRITIOF MODEL

In the course of a heavy-ion collision, the elementary hadron-hadron collisions happen at a finite baryon density. Therefore, the wave functions of incoming and outgoing

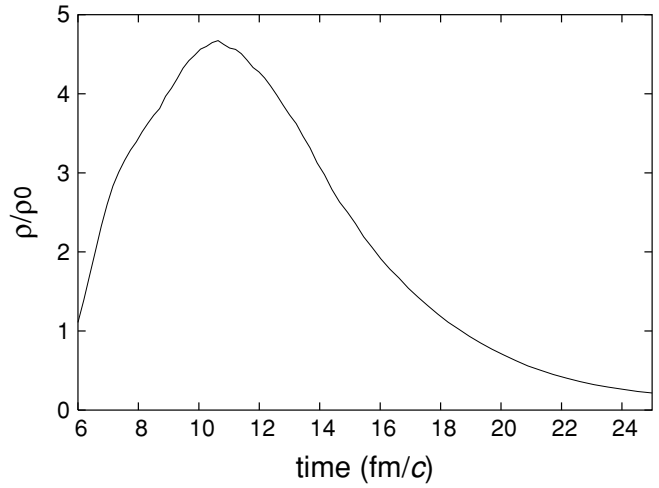

FIG. 24. Time evolution of the central baryon density in Au+Au collisions at 10.7A GeV, $b = 0$ fm.

particles are the in-medium plane waves rather than the vacuum ones.[2]

In order to take into account the in-medium modifications of the incoming and outgoing particles in the FRITIOF events, we follow here the approach of [29] generalized to the processes with many-meson final states. Only the events with two colliding nonstrange baryons will be modified. The in-medium modifications of the meson-baryon and meson-meson collisions are neglected, since as we expect, they are small with respect to the baryon-baryon case (see below).

Let us consider the process

$$B_1 B_2 \to B_3 B_4 M_5 M_6, \ldots, M_N, \tag{9}$$

where B_1, B_2 and B_3, B_4 are incoming and outgoing baryons, respectively; $M_5, M_6, \ldots, M_N$ are the produced mesons. The in-medium differential cross section of this process is given by the expression

$$d\sigma^{\rm med} = (2\pi)^4 \frac{(2m_1^*)(2m_2^*)(2m_3^*)(2m_4^*)}{4I^*} \overline{|T|^2} \times d\Phi_{N-2}(p_1^* + p_2^*; p_3^*, p_4^*, k_5^*, k_6^*, \ldots, k_N^*), \tag{10}$$

where $\overline{|T|^2}$ is the matrix element squared in the normalization of Ref. [30] averaged over spins of initial particles and summed over spins of final particles;

$$d\Phi_{N-2}(p_1^* + p_2^*; p_3^*, p_4^*, k_5^*, k_6^*, \ldots, k_N^*) = \delta^{(4)}(p_1^* + p_2^* - p_3^* - p_4^* - k_5^* - k_6^* - \cdots - k_N^*) \times \frac{d^3 p_3^*}{(2\pi)^3 2(p_3^*)^0} \frac{d^3 p_4^*}{(2\pi)^3 2(p_4^*)^0} \frac{d^3 k_5^*}{(2\pi)^3 2(k_5^*)^0} \cdots \frac{d^3 k_N^*}{(2\pi)^3 2(k_N^*)^0} \tag{11}$$

is the $(N-2)$-body phase space element [31] with $(p_i^*)^0 = [(\mathbf{p}_i^*)^2 + (m_i^*)^2]^{1/2}, i = 1, 2, 3, 4$ and $(k_i^*)^0 = [(\mathbf{k}_i^*)^2 + (m_i^*)^2]^{1/2}$, $i = 5, 6, \ldots, N$ being the zeroth components of the kinetic four-momenta, and the m_i^* being the effective (Dirac) masses of the particles involved. In Eq. (10), the flux factor is

$$I^* = q(\sqrt{s^*}, m_1^*, m_2^*)\sqrt{s^*}, \tag{12}$$

where $s^* \equiv (p_1^* + p_2^*)^2$ and

$$q(\sqrt{s^*}, m_1^*, m_2^*) = \{[s^* + (m_1^*)^2 - (m_2^*)^2]^2/(4s^*) - (m_1^*)^2\}^{1/2} \tag{13}$$

is the c.m. momentum of incoming baryons.

The matrix element $\overline{|T|^2}$ entering into Eq. (10) can be extracted from the vacuum cross section by dividing out the vacuum phase space and multiplying by the vacuum flux factor. Thus, our final result for the in-medium total cross section of the process (9) is

$$\sigma^{\rm med}(\sqrt{s^*}) = F\sigma^{\rm vac}(\sqrt{s}). \tag{14}$$

The modification factor F is

$$F \equiv \frac{m_1^* m_2^* m_3^* m_4^*}{m_1 m_2 m_3 m_4} \frac{I}{I^*} \frac{\Phi_{N-2}(\sqrt{s^*}; m_3^*, m_4^*, \ldots, m_N^*)}{\Phi_{N-2}(\sqrt{s}; m_3, m_4, \ldots, m_N)}, \tag{15}$$

where $I = q(\sqrt{s}, m_1, m_2)\sqrt{s}$. In Eq. (14), $\sqrt{s}$ is the c.m. energy of the colliding baryons in vacuum, which is directly provided by the BUU calculations in the cascade modus performed in the present work. The in-medium c.m. energy $\sqrt{s^*}$ is then determined from the condition that the energy excess above threshold is the same as in vacuum, i.e.,

$$\sqrt{s^*} = \sqrt{s} - m_3 - m_4 - \cdots - m_N + m_3^* + m_4^* + \cdots + m_N^*. \tag{16}$$

Since the modification factor F is proportional to the product of the ratios of the Dirac mass to the bare mass for incoming and outgoing fermions, we expect the meson-baryon and meson-meson channels to be modified relatively weaker.

In Eq. (10) we replaced the canonical four-momenta by the kinetic ones in the δ function entering the phase-space volume element (11). This is possible only if the vector fields cancel each other, which is valid in the case of the Walecka model (cf. Ref. [32]) but would be violated in a more sophisticated relativistic mean field model with momentum dependent scalar and vector fields [33]. Taking into account the momentum dependence, in particular for the vector field, which drops with momentum, is important for the description of the baryon flow in heavy-ion collisions above 1A GeV [34]. However, in the present exploratory work, we neglect the momentum dependence of the σ and ω fields, which would strongly complicate the calculation of the phase space volume.

We evaluate the in-medium masses using a nonlinear version NL2 [35] of the relativistic mean field model and assuming that the nucleons and all nonstrange baryonic resonances are coupled to the scalar mean field σ and to the vector mean field ω by the same universal coupling constants g_σ and g_ω [36]. This gives the Dirac effective masses

$$m_B^* = m_B + g_\sigma \sigma \tag{17}$$

[2]Exchange particles expressed by the propagators also get modified in-medium. However, this last effect would be strongly dependent on the model used for the description of an elementary collision. Thus, for simplicity, we neglect it by using the vacuum matrix elements in place of the in-medium ones.

and the kinetic four-momenta

$$p_B^* = p_B - g_\omega \omega \tag{18}$$

of the nonstrange baryons. The hyperon coupling constants are (cf. Ref. [32])

$$g_\sigma^Y = \tfrac{2}{3} g_\sigma, \quad g_\omega^Y = \tfrac{2}{3} g_\omega, \tag{19}$$

where $Y = \Lambda$ or Σ. The baryon single-particle energy is

$$\varepsilon(\mathbf{p}_B) = g_\omega \omega^0 + \sqrt{(\mathbf{p}_B^*)^2 + (m_B^*)^2}. \tag{20}$$

For the mesons π, ρ, and ω we neglect any in-medium modifications, while for the K and $\bar{K}$ single-particle energies we use the model of Refs. [38,37]:

$$\omega(\mathbf{k}, \rho) = \sqrt{(\mathbf{k}^*)^2 + (m_K^*)^2} \pm V^0, \tag{21}$$

where the upper (lower) sign corresponds to the K ($\bar{K}$) case;

$$\mathbf{k}^* = \mathbf{k} \mp \mathbf{V} \tag{22}$$

is the kaon kinetic momentum;

$$m_K^* = \sqrt{m_K^2 - \frac{\Sigma_{KN}}{f_\pi^2} \rho_s + V^2} \tag{23}$$

is the kaon effective (Dirac) mass; and

$$V^\mu = \frac{3}{8(f_\pi^*)^2} j^\mu \tag{24}$$

is the kaon vector field. ρ_s and j^μ are the scalar density and the baryonic four-current, respectively. The parameters which appear in Eqs. (23) and (24) are $\Sigma_{KN} = 450$ MeV, $f_\pi = 93$ MeV, and $(f_\pi^*)^2 = 0.6(f_\pi)^2$ [37]. Within these parameters, the following relation is expected to hold [37]:

$$V^\mu \simeq \tfrac{1}{3} g_\omega \omega^\mu. \tag{25}$$

Taking into account relations (19) and (25), one can see that the vector field is, indeed, completely excluded from the energy-momentum conservation conditions for strange particle production processes such as $B_1 B_2 \to B_3 Y_4 K$ or $B_1 B_2 \to B_3 B_4 K \bar{K}$, which provides the possibility of simplifying the in-medium calculations by just replacing the bare masses of particles by the Dirac masses, and the canonical four-momenta by the kinetic four-momenta.

We have calculated the modification factor $F(\sqrt{s}, \rho)$ as a function of the c.m. energy $\sqrt{s}$ and the baryon density ρ for various outgoing channels with no more than four mesons in the final state. We assume that the incoming baryons are nucleons, but an outgoing baryon can be either a nucleon or a Λ hyperon. For outgoing mesons, we have considered all possible combinations of pions, ρ mesons, kaons, and antikaons with no more than one kaon and one antikaon in the final state. The upper panel of Fig. 25 shows the medium modification factor $F(\sqrt{s}, \rho_0)$ for some selected processes: $NN \to NN\pi, NN\pi\pi, NN\rho, N\Lambda K, NNK\bar{K}$. We see that the modification factor depends on the outgoing channel rather weakly. In particular, the addition of a pion does not change the factor. In the lower panel of Fig. 25, we demonstrate the density dependence of the modification factor for the one-pion production channel. One can observe a strong decrease of the factor with the baryon density.

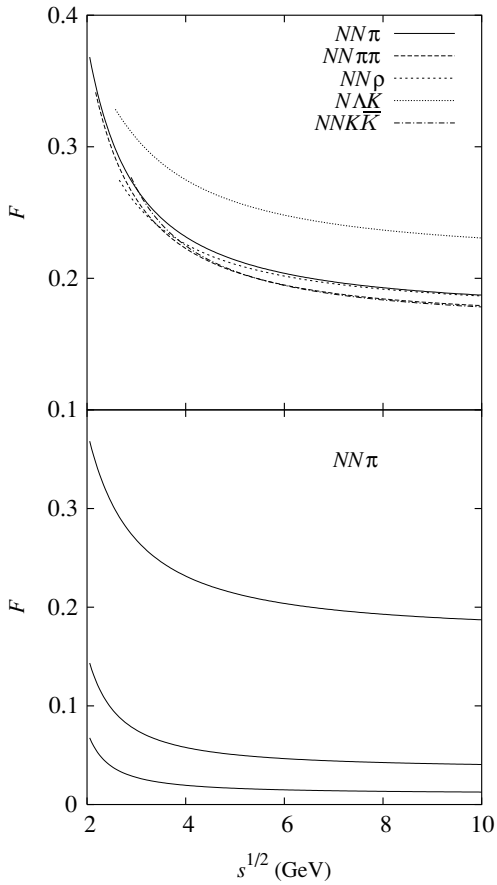

FIG. 25. In-medium modification factor F of the NN cross section vs. c.m. energy. Upper panel shows F at $\rho = \rho_0$ for various outgoing channels: $NN\pi$—solid line, $NN\pi\pi$—long-dashed line, $NN\rho$—short-dashed line, $N\Lambda K$—dotted line, and $NNK\bar{K}$—dash-dotted line. On the lower panel, the factor F is presented for the $NN\pi$ channel at $\rho = \rho_0, 2\rho_0$, and $3\rho_0$ in order from the upper to the lower line.

For the application to the FRITIOF model built in the BUU code, we have stored the factors F on a two-dimensional grid $(\sqrt{s}, \rho)$. Once some final state is generated by FRITIOF, it is accepted with the probability F. In the case where at least one of the incoming baryons is a resonance, we use the modification factor for incoming nucleons at the same $\sqrt{s}$. If an outgoing baryon is the Δ resonance, the factor for an outgoing nucleon is applied, shifted by the production threshold, i.e., $F(\sqrt{s} - m_\Delta + m_N)$. An analogous threshold correction is performed if Σ hyperon and/or K^* are produced.

In order to see an effect of the in-medium string model modifications in heavy-ion collisions, we have performed the calculation for the Au+Au system at 10.7A GeV. The results of this calculation are shown by the dashed lines in Figs. 9–14.

The proton rapidity spectra (Fig. 9) now get wider, in agreement with the experiment. This is expected since the inelastic NN cross section is reduced by the in-medium effects. The results with in-medium modifications for the most central events (upper left panel in Fig. 9) have a big statistical error due to a small number of events in this centrality class.

The π^+ rapidity spectra (Fig. 10) are reduced in closer agreement with the data, except for the very peripheral collisions. The K^+ rapidity spectra (Fig. 11) are also reduced. This, however, makes the agreement with the K^+ data worse.

The transverse mass spectra of π^+'s (Fig. 12) and K^+'s (Fig. 13) are reduced more at high transverse masses, since the high-$m_\perp$ particles are emitted from hard collisions which happen at the high baryon density where the in-medium modifications are stronger. Thus, the $m_\perp$-spectra get steeper, which, again, leads to a worse description of the K^+ data. The π^+'s transverse mass spectra at small $m_\perp$ are now better described, whereas at high $m_\perp$ the in-medium modifications result in a slight underestimation of the experiment.

Figure 14 summarizes our findings on the in-medium modifications. The π^+ fiducial yield is better described with the in-medium modifications, except for the very peripheral collisions. The K^+ fiducial yield is underestimated at all collision centralities with the in-medium modifications.

VI. SUMMARY AND OUTLOOK

In the present work, the BUU model developed earlier in Refs. [7,8] is further improved by including the heavy ($m > 2\,\mathrm{GeV}$) resonance or $q\bar{q}$-annihilation channel in the meson-baryon collisions and by the new meson-meson channels ($\pi\rho \to K\bar{K}$, $\rho\rho \to K\bar{K}$) for the strangeness production. Moreover, an in-medium modification of the FRITIOF model by taking into account the effective (Dirac) masses of the incoming and outgoing particles is formulated and implemented in BUU. The BUU model is applied to the nucleus-nucleus collisions at 2–40A GeV.

By performing a systematic study of the pion and kaon production for various systems and collision energies, we came to the following conclusions:

1. The $\pi^\pm$ and $K^\pm$ rapidity spectra and the inverse slope parameters of the transverse mass spectra from the proton-nucleus reactions are well described by BUU. The $q\bar{q}$-annihilation channel improves the agreement with the data on the K^+ production in proton-nucleus collisions (see Fig. 5).
2. In the peripheral Au+Au collisions at 10.7A GeV, the π^+ rapidity spectra are slightly underestimated, whereas the K^+ rapidity spectra are well described. This result is consistent with a good agreement between BUU and the data on the proton-nucleus reactions. The proton rapidity spectra are too narrow, i.e., the stopping power is overestimated by BUU, for all collision centralities.
3. In the central nucleus-nucleus collisions (Si+Au at 14.6A GeV/c, Au+Au at 2–10.7A GeV, and Pb+Pb at 30 and 40A GeV), the K^+ yields are, overall, well described, while the K^- and hyperon yields are somewhat overestimated. The π^+ yields are overestimated in all central heavy-ion collisions under study. The inverse slope parameters of the K^+ transverse mass spectra are strongly underestimated (Figs. 13 and 22). The pion slopes are well described (Fig. 12). Our BUU results on π^+ and K^+ agree, generally, with results of the HSD and UrQMD calculations from Refs. [6,21]. The excitation function of the K^+/π^+ ratio is described, however, better and closer to the thermal model results due to the introduction of the new meson-meson channels of the strangeness production, which increase the K^+ yield at the beam energy above 6A GeV (Fig. 19).
4. The in-medium modification of the FRITIOF model, which reduces the particle production cross sections, was tested for the system Au+Au at 10.7A GeV. This leads to the better description of the pion production, whereas the K^+ production is overdamped by the in-medium effects. The stopping power of the nuclear matter is reduced, which results in the better description of the proton rapidity spectra.

The K^+/π^+ ratio is quite sensitive to the meson-meson cross sections, and within the reasonable choice of these cross sections, we have decreased the discrepancy between BUU and the data by about a factor of 2. The resulting disagreement of $\sim$20% can thus hardly be considered a signal of the "new physics." The inverse slope parameter of the K^+ transverse mass spectra is a more serious problem for BUU. It would be worthwhile to study this topic in more detail by introducing, e.g., string-string and many-body collisions, which could both enhance the hard part of the kaon spectra.

ACKNOWLEDGMENTS

We thank W. Cassing for a careful reading of the manuscript and many helpful comments. We are also indebted to C. Greiner and E. Bratkovskaya for useful discussions and thank the latter for making the results of HSD and UrQMD calculations available to us. This work was supported by GSI Darmstadt.

[1] T. Abbott *et al.*, Phys. Rev. C **50**, 1024 (1994).
[2] J. Rafelski and B. Müller, Phys. Rev. Lett. **48**, 1066 (1982).
[3] S. Afanasiev *et al.*, Phys. Rev. C **66**, 054902 (2002).
[4] H. Sorge, Phys. Rev. C **52**, 3291 (1995).
[5] W. Cassing and E. Bratkovskaya, Phys. Rep. **308**, 65 (1999).
[6] H. Weber, E. Bratkovskaya, W. Cassing, and H. Stöcker, Phys. Rev. C **67**, 014904 (2003).
[7] M. Effenberger, E. Bratkovskaya, and U. Mosel, Phys. Rev. C **60**, 44614 (1999).
[8] M. Effenberger, Ph.D. thesis, University of Giessen, 1999, http://theorie.physik.uni-giessen.de/html/dissertations.html.
[9] L. Ahle *et al.*, Phys. Rev. C **59**, 2173 (1999).
[10] T. Falter, W. Cassing, K. Gallmeister, and U. Mosel, Phys. Rev. C **70**, 054609 (2004).
[11] B. Andersson, G. Gustafson, and H. Pi, Z. Phys. C **57**, 485 (1993).
[12] J. Geiss, W. Cassing, and C. Greiner, Nucl. Phys. **A644**, 107 (1998).

[13] G. Brown, C. Ko, Z. Wu, and L. Xia, Phys. Rev. C **43**, 1881 (1991).
[14] W. Cassing, E. L. Bratkovskaya, U. Mosel, S. Teis, and A. Sibirtsev, Nucl. Phys. **A614**, 415 (1997).
[15] H. Weber, Ph.D. thesis, University of Frankfurt, 2002.
[16] R. Mattiello, H. Sorge, H. Stöcker, and W. Greiner, Phys. Rev. Lett. **63**, 1459 (1989).
[17] T. Abbott, Phys. Rev. D **45**, 3906 (1992).
[18] Y. Pang, T. J. Schlagel, and S. H. Kahana, Phys. Rev. Lett. **68**, 2743 (1992).
[19] L. Ahle *et al*., Phys. Lett. **B476**, 1 (2000).
[20] L. Ahle *et al*., Phys. Lett. **B490**, 53 (2000).
[21] E. L. Bratkovskaya, S. Soff, H. Stöcker, M. van Leeuwen, and W. Cassing, Phys. Rev. Lett. **92**, 032302 (2004).
[22] P. Braun-Munzinger, J. Cleymans, H. Oeschler, and K. Redlich, Nucl. Phys. **A697**, 902 (2002).
[23] V. Friese, J. Phys. G **30**, S119 (2004).
[24] L. Tolos, A. Ramos, and A. Polls, Phys. Rev. C **65**, 054907 (2002).
[25] A. B. Larionov, W. Cassing, C. Greiner, and U. Mosel, Phys. Rev. C **62**, 064611 (2000).
[26] P. K. Sahu, A. Hombach, W. Cassing, M. Effenberger, and U. Mosel, Nucl. Phys. **A640**, 493 (1998).
[27] W. Cassing, Nucl. Phys. **A700**, 618 (2002).
[28] E. L. Bratkovskaya, M. Bleicher, M. Reiter, S. Soff, H. Stöcker, M. van Leeuwen, S. A. Bass, and W. Cassing, Phys. Rev. C **69**, 054907 (2004).
[29] A. B. Larionov and U. Mosel, Nucl. Phys. **A728**, 135 (2003).
[30] J. D. Bjorken and S. D. Drell, *Relativistic Quantum Mechanics* (McGraw-Hill, New York, 1964).
[31] K. Hagiwara *et al*., Phys. Rev. D **66**, 010001 (2002).
[32] X. S. Fang, C. M. Ko, G. Q. Li, and Y. M. Zheng, Phys. Rev. C **1994**, 608 (1994).
[33] K. Weber, B. Blättel, W. Cassing, H. C. Dönges, V. Koch, A. Lang, and U. Mosel, Nucl. Phys. **A539**, 713 (1992).
[34] P. K. Sahu, A. Hombach, W. Cassing, M. Effenberger, and U. Mosel, Nucl. Phys. **A640**, 493 (1998).
[35] S. Lee *et al*., Phys. Rev. Lett. **57**, 2916 (1986).
[36] K. Wehrberger, C. Bedau, and F. Beck, Nucl. Phys. **A504**, 797 (1989).
[37] G. Brown and M. Rho, Nucl. Phys. **A596**, 503 (1996).
[38] Yu-Ming Zheng, C. Fuchs, Amand Faessler, K. Shekhter, Yu-Peng Yan, and Chinorat Kobdaj, Phys. Rev. C **69**, 034907 (2004).
[39] A. Baldini, V. Flaminio, W. G. Moorhead, and D. R. O. Morrison, *Landolt-Börnstein* (Springer-Verlag, Berlin, Heidelberg, 1988),Vol. 12a.
[40] A. Mischke *et al*., J. Phys. G **28**, 1761 (2002).
[41] A. Mischke *et al*., Nucl. Phys. **A715**, 453 (2003).
[42] S. Ahmad *et al*., Phys. Lett. **B382**, 35 (1996).
[43] C. Pinkenburg, Nucl. Phys. **A698**, 495 (2002).
[44] F. Antinori, Nucl. Phys. **A661**, 130 (1999).